Compositionally stratified cratonic lithosphere: petrology and geochemistry of peridotite xenoliths from the Labait tuff cone, Tanzania

Lee, C-T *and Rudnick, R L, 1999, Compositionally stratified cratonic lithosphere: petrology and geochemistry of peridotite xenoliths from the Labait tuff cone, Tanzania. In J J Gurney and S R Richardson (eds). Proceedings of the 7th International Kimberlite Conference, pp 503-521.*

Compositionally Stratified Cratonic Lithosphere: Petrology and Geochemistry of Peridotite Xenoliths from the Labait Volcano, Tanzania

C.-T. LEE and R.L. RUDNICK

Department of Earth and Planetary Sciences, Harvard University, Cambridge, MA 02138, USA

ABSTRACT

In northern Tanzania, manifestations of the East African Rift, such as crustal warping, rifting, and magmatism, are currently propagating into the margins of the Archean Tanzanian craton. In order to understand the factors that govern the origin and stability of cratonic mantle, we are studying peridotite xenoliths from the Quaternary Labait volcano, located on the northeastern edge of the craton. We find that refractory mantle (Mg# up to 92) persists to depths of at least 150 km, with a marked increase in fertility at depths > 120 km. This compositional stratification may be due to 1) an original variation in depth of degree of partial melting, 2) refertilization from below of a preexisting depleted mantle section, or 3) incremental downward growth of the lithosphere with time. Re-Os systematics favor the latter two hypotheses (Chesley *et al.*, 1998).

The refractory peridotites are less dense than pyrolite, and the preservation of old Re-Os ages beneath Labait attests to the perseverance of cratonic mantle despite proximity to rifting. However, high proportions (75 %) of dense, Fe-rich (Mg# < 88) dunites in the xenolith population and elevated temperatures at depth indicate that chemical and thermal interaction of the mantle section with asthenospheric magmas has and is occurring. Collectively, these features result in slow shear-wave velocities, consistent with the results of a recent seismic tomographic study, which shows that the effects of rifting are beginning to propagate into the cratonic mantle beneath Labait.

Keywords: xenolith, mantle, stratification, craton, density, delamination, stability, refractory, isopycnic

1. INTRODUCTION

Geologic and geochemical studies of mantle xenoliths suggest that cratons are underlain by an anomalously thick, cold mantle keel (Jordan, 1978; Boyd, 1989a), which can be stable over timescales greater than two billion years (Richardson *et al.*, 1984; Walker *et al.*, 1989; Pearson *et al.*, 1995). Cooler temperatures should increase density and hence decrease the buoyancy of mantle peridotite; if cold enough, entrainment into the convecting mantle would be expected. The observed longevity of cratonic mantle beneath Archean shields, however, requires an additional factor that compensates for the increased density caused by colder temperatures. One possibility is that cratonic mantle is intrinsically less dense than the surrounding mantle due to its more depleted chemical composition (Ringwood, 1966; Jordan, 1978), leading to the popular notion that cratonic keels are regions of tectonic stability immersed within a mobile and actively convecting mantle.

To determine how cratonic mantle is generated, stabilized, and potentially destabilized, we are conducting an integrated petrographic and geochemical study of mantle xenoliths from the Labait volcano, located on the northeastern margin of the Tanzanian craton. Because the Tanzanian craton is located within an intracontinental rift, our results have implications for the effects of rifting on cratonic mantle. In addition, there are ongoing geophysical studies in the same region (Ritsema *et al.*, 1998), providing an unique opportunity to make direct comparisons between geophysical and geochemical datasets. Here, we show that the Tanzanian mantle is compositionally stratified, with a step-wise increase in fertility with depth. We also show that local Fe-enrichment is superimposed on the overall compositional stratigraphy and that dense, Fe-rich peridotites are the dominant xenolith types at Labait. We discuss the implications of these findings for the origin and potential demise of cratonic mantle.

2. REGIONAL GEOLOGY

The Tanzanian craton is an amalgamation of several Archean granitoid terranes, which formed primarily during three short periods (~2.9, ~2.7, and ~2.4 Ga) based on Sm/Nd, Rb/Sr, and U-Pb dating (Pinna *et al.*, 1996). In the northern portion of the craton, these granitoids intrude and separate many large and small greenstone belts (Borg and Shackleton, 1997). Re-Os depletion ages for mantle xenoliths from Labait yield minimum melt extraction ages of up to ~2.8 Ga, indicating that stabilization of the lithospheric mantle occurred by the end of the Archean (Chesley *et al.*, 1998). The craton is surrounded by several Proterozoic mobile belts. It is bounded to the east by the polycyclic collisional Mozambique belt (900-500 Ma), which consists of a region of reworked Archean crust directly east of the craton (based on Sm-Nd model ages; Möller *et al.*, 1998), and a region of younger, accreted crust further east and northeast (Pinna *et al.*, 1996; Möller *et al.*, 1998). To the east and southeast, the craton is bounded by the Usagaran Belt, which is a Proterozoic subduction zone (based on U-Pb dates of metamorphic minerals from eclogite facies rocks (Möller *et al.*, 1995)). To the southwest, the craton is bounded by the Early to Middle Proterozoic Ubendian Belt (2.0 Ga), to the west by the Late Proterozoic Karagwe-Ankolean Belt and the early Paleozoic Bukoban system, and to the northwest by the Ruwenzori Belt of Uganda.

In northern Tanzania, Cenozoic tectonism is dominated by rifting. The Eastern Branch of the East African Rift system, the Gregory Rift, is composed of three distinct rifts, the NW-trending Pangani rift, the N-S-trending Natron-Manyara-Balangida rift, and the NE-trending Eyasi-Wembere rift. The latter two rifts transect the boundary between Archean and Proterozoic crust (Ebinger *et al.*, 1997; Foster *et al.*, 1997). The present rift basins and volcanism are mostly younger than 2 Ma, with ages not exceeding 4 Ma (Dawson, 1992). The xenolith locality, Labait, is an olivine-melilitite volcano (4° 34'S, 35° 26'E) composed of flows and tuffaceous units and located in the Tanzanian section of the East African Rift, south of Mount Hanang on the northeastern edge of the Tanzanian craton (Dawson *et al.*, 1996). The eruption age is constrained to be Quaternary by U-Pb dating of metasomatic zircons in a mantle xenolith (Rudnick *et al.*, 1998).

Geophysically, the Tanzanian craton is characterised by high elevation, a negative Bouger gravity anomaly (Ebinger *et al.*, 1997), and low surface heat flow (Nyblade *et al.*, 1990). Results from a recent broad-band seismic experiment show that the Tanzanian mantle root is largely intact beneath the craton, that the uplift and negative gravity anomaly are due to hot, low density material beneath the cratonic root, and that erosion and/or heating of this ancient root is confined to the vicinity of the rift (Ritsema *et al.*, 1998).

3. OVERVIEW OF XENOLITH SUITES

To estimate the proportions of various xenolith types, we systematically collected all xenoliths encountered during the first half day of fieldwork (n = 117). Fe-rich dunites make up ~75% of the Labait xenoliths and were identified in the field by the dark green color of their olivine. Of these, 25% contain visible chrome diopside in hand-specimen. Residual peridotites make up 22% of the xenoliths and were identified by their light-green olivines. The remaining <3% consist of lower crustal xenoliths (granulites), glimmerites, and pyroxenites. In this paper, we focus on a smaller selection of samples, which consists of 38 residual peridotites, nine Fe-rich dunites, one wehrlite, and one glimmerite. Six garnet-bearing peridotites from Dawson *et al.* (1996) are also included. Modal mineralogies are shown in Fig. 1 and reported in Table 1. Xenolith sizes range from 5 to 30 cm in diameter and are mostly egg-shaped. Unlike kimberlite-hosted xenoliths, which are often heavily serpentinized, the Labait peridotite xenoliths are serpentine-free and generally fresh.

Residual peridotites are harzburgites or clinopyroxene-poor lherzolites, and contain either hercynitic spinel, chromite, or garnet. We have classified these peridotites into garnet and spinel facies based on the presence of garnet or, in the absence of garnet, on spinel and orthopyroxene chemistry and calculated temperatures of equilibration. The Fe-rich dunites can contain Cr-diopside, chromite, or both. Wehrlites are also Fe-rich (LB15) and can occur as cross-cutting planar dikes in composite xenoliths (e.g. LB19). Only one glimmerite was collected. This sample consists of fine-grained phlogopite grains with interstitial ilmenites.

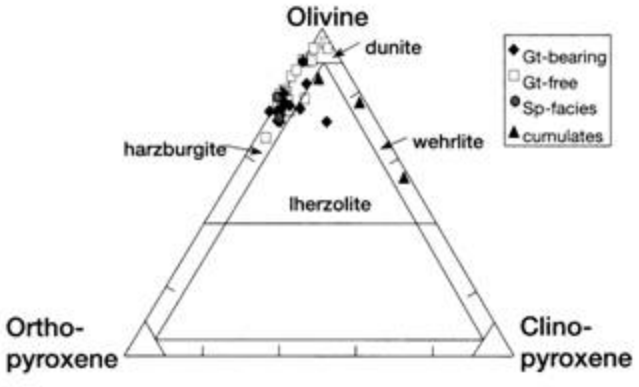

Figure 1. Modes calculated by least-squares regression of whole-rock and mineral elemental analyses for Labait peridotites (garnet and spinel normalized out). Garnet-free peridotites refer to peridotites containing chromite and low Al_2O_3 orthopyroxene and are distinct from true spinel-facies peridotites.

Table 1.

	Modal Mineralogy*						
	OL	CPX**	OPX	SP	PHL	GT	Trace***
Garnet-Lherzolites							
LB 12	70.1	7.0	15.3			7.6	Sf
LB 45	60.8	14.0	9.8			15.4	
Garnet Harzburgites							
LB 4	68.2	4.1	22.5			5.1	Sf
LB 2	72.1	2.1	22.0	3.8			
LB 24	76.9	1.0	17.6			4.5	Sf
LB 34	88.2	1.1	8.2			2.6	Ph
LB 50-1	72.8	2.5	20.3			4.4	Sf
LB 53	77.3	5.1	10.2			7.5	Sf
KAT 17	72.0	3.5	24.1			0.4	
GL4202	73.7	4.2	18.0			4.2	
GL4203	75.2	1.8	18.9			4.1	
GL4206	71.2	0.0	23.6			5.2	
Garnet-free Peridotites							
KAT 1	67.8	1.1	28.2	2.8			
LB 1	77.7		20.6	1.7			Sf, Ph
LB 6	86.9	(2.22)	6.8	2.4	1.7		Sf
LB 7	87.9	(0.68)	8.0	3.4			Sf, Ph
LB 8	79.9	(0.54)	17.3	2.3			Sf, Ph
LB 9	76.7	(7.03)	13.4	2.8			Ilm
LB 14	94.4	1.9	3.7				Ph
LB 16	78.4	1.3	19.4	0.9			Sf, Ph, Hm
LB 17	75.0	1.1	21.7		4.5		Sr, Rt, Zr
LB 21	96.1	(3.94)		tr			Sf, Ph, Rt, Pv
LB 22	77.6	1.5	18.2	2.7			Sf, Ph, Pv
LB 23	79.6	1.5	17.1	4.3			Sf, Ph, Rt, Pv
LB 26	85.9	0.3	13.8				Sf, Pv
LB 32	77.5	3.1	18.2	1.2			Sf, Ph, Pv
LB 33	86.4	3.1	5.8		4.7		Sf, Ph, Rt, Pv
LB 36	73.9	(2.62)	21.9	1.6			Sf
LB 39	63.3	2.9	28.3	5.4			
LB 40	79.4		19.4	1.2			Ilm
LB 54	73.8	5.1	19.1	2.0			Sf, Ph
LB 55	75.7	1.6	19.9	2.7			Sf, Ph
LB 60	79.2	0.9	17.8	1.2	1.0		Sf, Ph
LB 61	86.5	(0.63)	11.4	0.8	0.7		
Spinel-facies Peridotites							
LB 11	78.6	0.8	19.5	1.2			Sf
LB 29	78.4		20.3	1.4			Pv
LB 31	69.7	3.4	22.2	4.7			Sf
Fe-rich Dunites & Wehrlites							
LB 15	54.8	45.2					
LB 46	83.7	7.7	6.9	1.7			Ilm
LB 51	75.6	21.4		2.9			
LB 58	92.3	5.4		2.3			Crbn, Nph
LB 59	95.9				4.1		

* all modes have been normalized to 100 after least squares fitting
** Parentheses around secondary clinopyroxenes
*** 3rd column represents trace metasomatic phases not included in calculations
Sf=Sulfide; Rt=Rutile; Ph=Phlogopite; Zr=Zircon; Pv=Perovskite
Ilm=Ilmenite; Nph=Nepheline; Crb=Carbonate; Hm=Harmatome
LB 4 = calculated using garnet from LB 12
LB 17 = pervasive veining giving rise to poor least square fits
LB 34 = calculated using garnet from LB 12
LB 39 = calculated assuming no phlogopite
LB 50-1 = calculated using garnet from LB 12
GL's = data from Dawson *et al.* (1996)

4. PETROGRAPHY

4.1 Olivine

Olivines are fresh and range from fine-grained and equant to coarse-grained and tabular in shape. Undulose extinction due to kink-banding is observed in many samples. Mosaic-porphyroclastic texture, reminiscent of Kaapvaal high temperature sheared peridotites, is typical of the garnet-bearing and higher temperature peridotites at Labait. In these xenoliths, there are sometimes two textural generations of olivine. One generation is characterized by small equant grains, which show varying degrees of grain boundary recrystallization. The other generation consists of larger olivine grains, which have a more tabular morphology, perhaps formed by partial annealing (Mercier, 1985). Olivine inclusions occasionally occur in garnet breakdown patches. Similar inclusions have been observed in fresh garnets from the Lashaine xenolith site, located approximately 150 km northeast of Labait (Rudnick *et al.*, 1994).

4.2 Orthopyroxene

Orthopyroxenes occur as small to large groundmass grains and also as products of garnet breakdown. Exsolution lamallae are confined to orthopyroxenes from spinel-facies xenoliths. In one sample (LB17), orthopyroxene is more abundant in a late-stage metasomatic vein that also includes zircon, rutile, phlogopite, sulfides, and ilmenite.

4.3 Clinopyroxene

Clinopyroxene commonly occurs as a secondary phase, where it rims chromite and orthopyroxene, in garnet breakdown patches, and in metasomatic veins and patches. These clinopyroxenes are characterised by small grain size and poorly developed morphology, typically appearing as amorphous interstitial blebs. Clinopyroxene also occurs as larger primary grains in wehrlites, Fe-rich cumulates, and in garnet-bearing peridotites; these have better developed morphology compared to secondary grains.

4.4 Garnet

Garnets occur as discrete, round grains. All garnets (except for those in LB2) have a two-stage decomposition history based on the occurrence of texturally distinct outer and inner breakdown assemblages (Fig. 2a). The outer assemblage is coarser-grained than the inner assemblage and resembles coronas developed around garnets in crustal metamorphic rocks. These coronas consist of equidimensional grains of symplectic pale-brown spinel, orthopyroxene, and clinopyroxene (fine-grained) which embay the surrounding groundmass olivines. Phlogopite and sulfide occasionally occur as accessory phases (e.g. LB12, 34). In most samples, the petrography and textures suggest the following reaction: gt + ol = opx + sp + cpx (Reid and Dawson, 1972; Smith, 1977; Jaques *et al.*, 1990). The occasional presence of sulfide and phlogopite in some of the garnet coronas shows that the process was not entirely isochemical.

The interiors of former garnets consist of very fine-grained kelyphite encased by the outer corona assemblage (Fig. 2a, b). Pristine garnet, if present, occurs at the center of these fine-grained cores or as tiny grains distributed within the inner kelyphite. In thin section, the inner kelyphite appears as an aphyric, feathery-textured mass. In some samples, the aphyric mass is composed of smaller, round subdomains with radiating fabric, which are remarkably homogeneous in back-scattered electron images, but which contain small amounts of Na, indicating that the kelyphite formation was not entirely isochemical.

In the breakdown assemblages described above, no glass was found. However, in LB2 there are round to oval-shaped patches consisting of clinopyroxene, orthopyroxene, glass (fresh), and occasionally olivine. Clinopyroxene and glass are the dominant phases, with clinopyroxene occurring as small

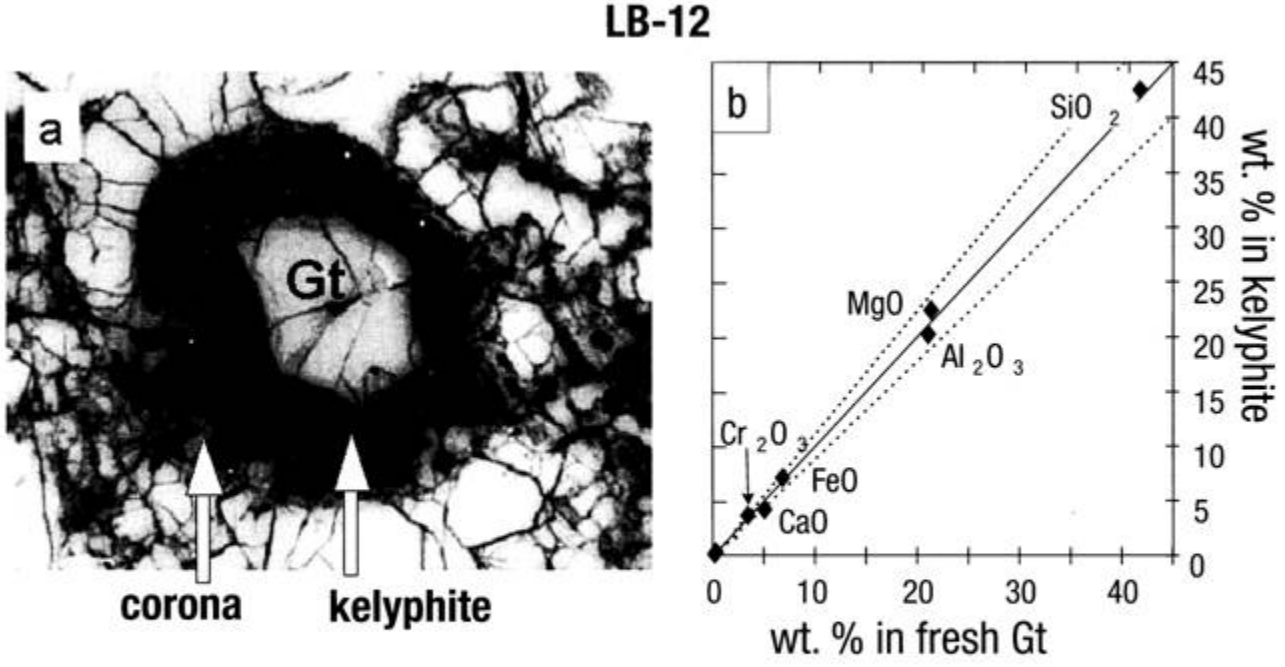

Figure 2. **(a)** Photomicrograph of a partially decomposed garnet in LB12 (plane-polarized light). Note that the fresh garnet core (clear) is enclosed by an outer coronal assemblage, consisting of aluminous spinel, orthopyroxene, and clinopyroxene grains, which itself encloses an inner kelyphite assemblage, characterized by a fine-grained aphyric mass. **(b)** Rastered probe analyses of the inner kelyphite assemblage versus that of the fresh garnet. Symbol in lower left corner is TiO_2. Dotted lines represent 10% deviation from 1:1 (solid line).

grains separated by thin glass films, resulting in a fishnet-like texture. In some cases, clinopyroxene aggregates within a single patch exhibit identical extinction. The glass and clinopyroxene also embay or intrude into the olivine wallrock, imposing a serrated appearance to the olivine grain boundaries. We interpret these patches also as former garnets.

4.5 Chromite and Spinel

Chromite or spinel is observed in almost all samples, with variations in composition and texture between samples. Chromite is generally opaque while spinels tend to be reddish-brown. Chromites are scarce in garnet-bearing peridotites, but aluminous spinels occur in the garnet breakdown patches. In harzburgites, chromite occurs as large, round blebs which form in the interstices of the primary mineral assemblage or as inclusions in olivine or orthopyroxene; these are presumed to be primary. The latter occasionally induce radial fractures in their host mineral. Chromites also occur as irregular, skeletal growths, which have distinct "herring-bone" textures. Many of the chromites appear to be mantled by secondary mineral assemblages. In harzburgites, some chromites have thin rims of rutile, which may have formed by exsolution of Ti during cooling or by precipitation from a Ti-rich metasomatic fluid (Bodinier *et al.*, 1996). Late-stage metasomatic selvages consisting of clinopyroxene, phlogopite, and/or other phases may also mantle these primary chromites. In one Fe-rich sample, LB58, plate-like chromites are mantled by clinopyroxene, carbonate, glass, and other secondary minerals (Lee and Rudnick, 1998). Similar observations have been reported from other xenolith suites and attributed to carbonatite-metasomatism (e.g. Dautria *et al.*, 1992; Rudnick *et al.*, 1993).

4.6 Phlogopite

Phlogopite occurs mostly as a secondary phase, associated with metasomatic veins or patches but only rarely as a texturally primary phase. For example, in LB19C it occurs as large platy grains within the groundmass olivine. In this particular specimen, small skeletal chromites are included within the phlogopites.

4.7 Other minerals

In several samples, sulfides occur in association with metasomatic and garnet breakdown patches and as tiny inclusions in olivine or on grain boundaries. Other metasomatic phases such

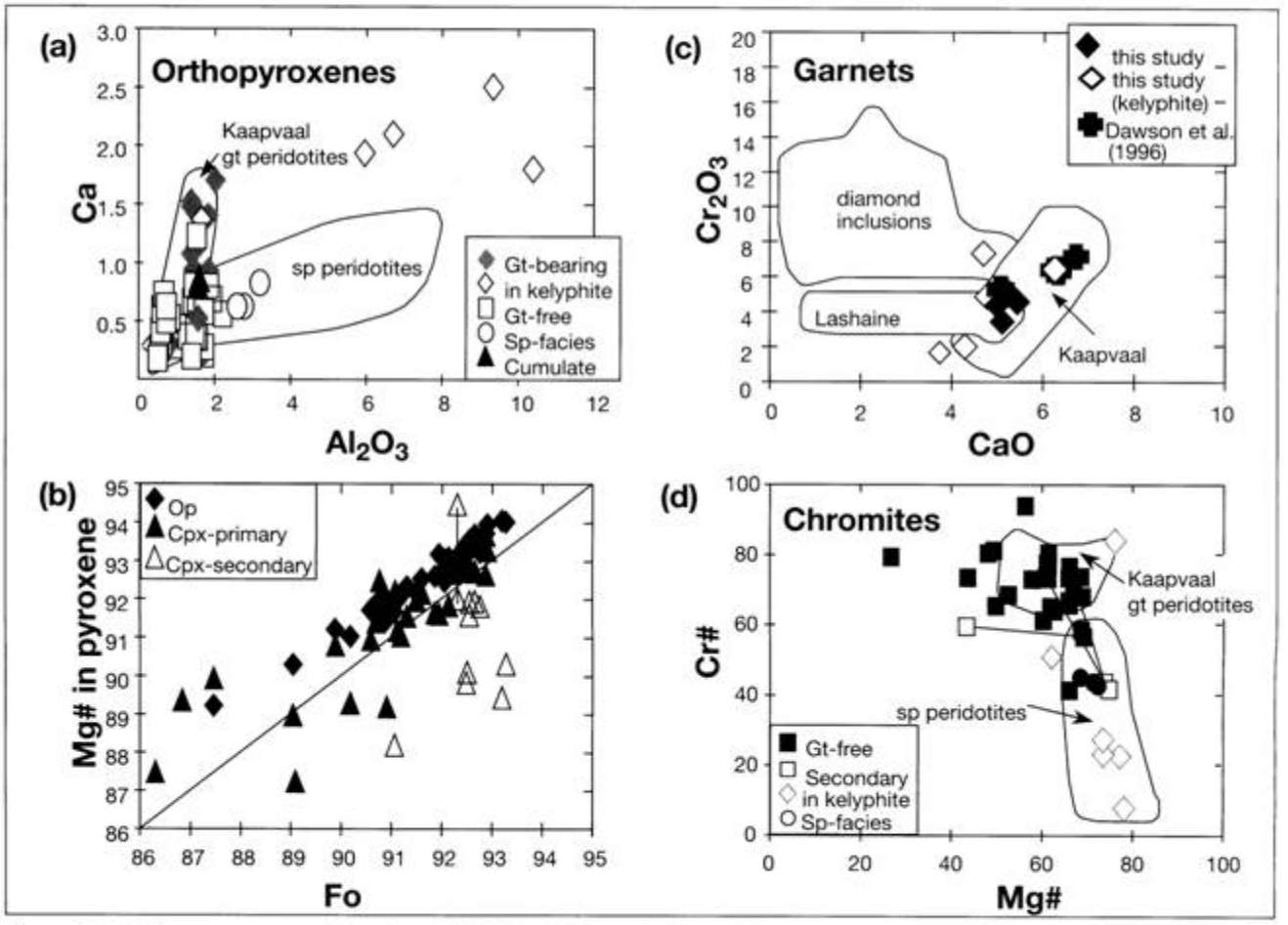

Figure 3. **(a)** Orthopyroxene compositions plotted with field of spinel peridotites and Kaapvaal garnet peridotites. Note the three samples with high Al_2O_3 (grey circles), which are true spinel-facies peridotites. Open diamonds represent kelyphitic orthopyroxenes associated with garnet breakdown. **(b)** Mg# (=100 Mg/Mg+Fe) of pyroxenes in all samples plotted against forsterite content of coexisting olivines. Solid line represents 1:1 correspondence. Orthopyroxenes exhibit a tight correlation, whereas clinopyroxenes are highly scattered. Those that plot well-below the 1:1 line are not in equilibrium with the primary assemblage. Tieline connects two generations of clinopyroxene in one sample. **(c)** Garnet compositions compared to fields of Kaapvaal garnet peridotites, inclusions in diamonds, and Lashaine garnet peridotites. Open diamonds represent compositions measured from rastered probe analyses of fine-grained kelyphites in samples where fresh garnet is absent. **(d)** Chromite composition compared to field of spinel peridotites and Kaapvaal garnet peridotites. Tielines connect two generations of chromite in the same sample.

Table 2.

	Garnet Lherzolites													Garnet Harzburgites				
	LB12					LB-45								KAT-17				
	opx	cpx	gt	gt klyphte	ol	opx	opx klyphte	cpx core	cpx rim	gt klyhpte	sp klyphte	ol matrix		opx	cpx core	cpx rim	gt	ol
SiO_2	56.73	54.23	41.83	42.54	40.04	55.96	52.70	54.18	52.77	42.40	0.15	40.27		56.11	53.71	53.54	41.78	39.82
TiO_2	0.07	0.14	0.21	0.17	0.02	0.20	0.19	0.38	0.42	0.73	0.22	0.03		0.17	0.49	0.43	0.25	0.03
V_2O_5											0.11							
Al_2O_3	1.51	2.74	21.08	20.17	0.04	2.02	6.72	3.45	3.72	21.52	60.57	0.06		1.56	3.10	2.71	19.76	0.02
Cr_2O_3	0.39	1.20	3.46	3.65	0.05	0.30	0.62	0.65	0.75	2.06	7.84	0.05		0.47	1.61	1.81	5.14	0.03
FeO	5.51	3.32	6.84	7.07	8.99	5.78	6.39	4.35	4.18	7.05	10.76	9.60		6.41	3.79	3.82	6.96	10.46
MnO	0.12	0.11	0.30	0.29	0.11	0.11	0.23	0.12	0.12	0.25	0.18	0.09		0.13	0.10	0.11	0.28	0.13
MgO	34.27	18.72	21.35	22.42	48.70	32.94	30.63	20.35	20.28	21.57	21.43	49.47		33.52	17.18	17.63	20.90	47.68
NiO					0.36						0.08	0.36						0.37
CaO	1.11	17.02	5.08	4.19	0.09	1.70	2.10	13.78	15.95	4.29	0.00	0.12		0.29	16.70	16.92	5.23	0.05
Na_2O	0.24	1.74		0.17		0.30	0.10	1.82	0.83	0.29					0.29	2.21	1.86	
K_2O																		
F																		
Cl																		
Total	99.95	99.22	100.15	100.67	98.40	99.31	99.68	99.08	99.02	100.16	101.35	100.05		98.95	98.89	98.83	100.30	98.59
Cr/Cr+Al											7.99							
Mg/Mg+Fe	91.72	90.95	84.77	84.97	90.62	91.03	89.52	89.29	89.64	84.51	78.03	90.18		90.31	88.99	89.16	84.26	89.04

	Garnet Harzburgites																		
	LB-2								LB-4						LB-24				
	opx core	opx rim	cpx	cpx symp	sp	sp symp	ol matrix	ol symp	opx	opx gt inclsn	cpx	gt klphyte	sp klyphte	ol matrix	opx	cpx	gt	gt	sp klyphte	ol klyphte
SiO_2	57.44	56.61	53.53	52.69	0.05	0.15	40.79	41.41	56.81	57.00	54.49	41.48	0.09	40.63	56.91	53.91	41.96	38.60	0.12	40.66
TiO_2	0.04	0.05	0.15	0.33	0.25	0.74	0.00	0.00	0.05	0.04	0.09	0.19	0.01	0.01	0.09	0.18	0.29	0.26	0.11	0.01
V_2O_5					0.15	0.17							0.09						0.11	
Al_2O_3	0.83	1.56	4.48	3.14	23.37	19.91	0.02	0.06	1.69	1.66	2.61	19.93	2.62	0.03	1.45	2.84	20.28	18.16	48.04	0.04
Cr_2O_3	0.26	0.36	2.11	2.15	45.57	43.80	0.02	0.11	0.51	0.54	1.22	4.91	21.53	0.07	0.56	1.86	4.90	5.80	21.48	0.05
FeO	4.29	4.43	2.28	1.91	13.59	23.57	6.97	5.08	5.06	5.11	3.25	6.11	10.65	8.45	4.51	2.52	5.78	6.34	10.38	7.36
MnO	0.10	0.11	0.09	0.05	0.10	0.54	0.12	0.08	0.10	0.12	0.10	0.25	0.16	0.11	0.10	0.10	0.25	0.26	0.29	0.11
MgO	35.99	35.49	16.10	18.09	17.07	10.11	50.92	52.10	34.23	34.44	19.80	22.43	19.48	49.82	34.80	18.18	21.71	23.51	19.51	50.71
NiO					0.15	0.06	0.42	0.42					0.00	0.38					0.06	0.39
CaO	0.30	0.55	18.52	20.61	0.00	0.14	0.06	0.18	0.22	1.37	16.55	4.77	0.00	0.13	0.94	17.37	5.04	1.92	0.04	0.07
Na_2O	0.07	0.14	2.22	0.74					0.22	0.25	1.45	0.03			0.22	1.85		0.04		
K_2O																				
F																				
Cl																				
Total	99.32	99.30	99.48	99.71	100.32	99.27	99.32	99.44		98.89	100.53	99.56	100.10	54.65	99.63	99.58	98.81	100.21	94.90	100.14
99.40																				
Cr/Cr+Al					56.67	59.61							84.65						23.07	
Mg/Mg+Fe	93.73	93.45	92.64	94.41	69.13	43.33	92.87	94.81	92.34	92.31	91.57	86.75	76.53	91.31	93.22	92.79	87.00	86.85	77.02	92.47

Table 2. cont.

Garnet Harzburgites

	LB-34									LB-50				LB-53					
	opx	cpx	gt klyphte	sp p	sp klyphte	sp klyphte	ol	ol gt inclsn	phlog klyphte	opx	cpx	gt klyphte	ol	opx	cpx	gt	gt klyphte	sp klyphte	ol
SiO_2	56.47	52.00	38.84	0.31	0.70	0.25	40.43	40.88	39.03	56.31	54.38	42.98	40.29	57.16	54.35	41.39	40.51	0.32	40.80
TiO_2	0.22	1.35	0.07	4.74	0.23	2.30	0.03	0.01	3.33	0.09	0.18	0.31	0.02	0.23	0.38	0.71	0.62	0.39	0.03
V_2O_3				0.31	0.07	0.18												0.10	
Al_2O_3	1.61	1.96	18.26	13.40	43.75	24.95	0.03	0.08	13.44	1.83	2.92	21.96	0.05	1.54	2.60	19.42	19.00	46.71	0.03
Cr_2O_3	0.56	1.28	7.31	43.63	24.84	39.28	0.04	0.10		0.36	0.73	1.73	0.04	0.53	1.51	4.72	5.05	21.56	0.06
FeO	5.79	3.19	6.01	22.95	11.92	17.06	9.79	7.36	4.61	5.21	3.52	6.44	8.49	5.35	3.23	6.70	7.15	12.05	8.67
MnO	0.11	0.10	0.33	0.30	0.30	0.37	0.12	0.10	0.02	0.10	0.10	0.24	0.12	0.10	0.09	0.28	0.30	0.28	0.12
MgO	33.72	17.65	21.86	14.22	18.45	15.48	49.03	50.49	22.16	34.04	20.12	23.56	49.53	34.41	18.76	20.90	23.28	18.67	49.92
NiO				0.33	0.07	0.25	0.35	0.38					0.39					0.08	0.38
CaO	0.78	20.45	4.74	0.03	0.04	0.03	0.05	0.05	0.01	1.40	16.01	3.72	0.11	1.19	17.21	5.42	4.05	0.03	0.08
Na_2O	0.27	0.69	0.39						0.27	0.26	1.46	0.06		0.24	1.67	0.06	0.11		
K_2O									10.09										
F									0.52										
Cl									0.02										
Total	99.53	98.67	97.81	100.25	100.37	100.17	99.87	99.45	100.00	99.60	99.42	101.00	99.04	100.75	99.80	99.60	100.07	100.19	100.09
Cr/Cr+Al				68.60	27.58	51.37												23.64	
Mg/Mg+Fe	91.21	90.80	86.64	52.49	73.40	61.80	89.93	92.44	89.55	92.09	91.06	86.71	91.23	91.97	91.19	84.76	85.30	73.42	91.12

Garnet-free Peridotites

	KAT 1					KAT 4				KAT 8						LB-1			
	opx	cpx patch	sp	ol matrix	ol patch	cpx patch	sp	ol matrix	ol patch	opx	cpx core	cpx rim	sp core	sp rim	ol	opx	sp	sp 2ndry	ol
SiO_2	57.85	53.21	0.07	40.96	40.95	49.21	0.06	43.72	40.91	57.17	53.23	53.50	0.11	0.15	41.25	57.89	0.07	0.20	40.83
TiO_2	0.07	1.34	1.19	0.02	0.02	1.47	0.32	0.01	0.01	0.03	0.14	0.15	0.18	4.54	0.01	0.03	0.51	2.02	0.01
V_2O_3							0.18						0.17	0.24			0.18	0.57	
Al_2O_3	1.33	0.97	14.50	0.01	0.01	6.19	31.24	0.51	0.07	1.71	3.59	3.48	32.51	10.53	0.01	0.61	13.57	31.65	0.02
Cr_2O_3	0.40	0.41	51.95	0.05	0.11	0.75	36.99	0.11	0.20	0.25	0.97	0.78	35.60	43.51	0.04	0.19	55.93	36.61	0.01
FeO	4.50	3.99	16.25	7.30	7.34	2.66	13.24	6.93	5.75	4.99	2.64	2.93	13.86	24.85	7.77	4.43	13.66	11.77	7.13
MnO	0.10	0.09	0.19	0.09	0.11	0.00	0.15	0.12	0.10	0.13	0.09	0.11	0.16	0.30	0.11	0.12	0.22	0.11	0.10
MgO	36.01	16.81	15.31	50.67	50.56	15.70	17.72	47.20	51.46	35.59	17.86	18.55	17.43	13.75	50.54	36.51	15.41	18.50	50.76
NiO				0.39	0.29		0.24	0.35	0.38				0.20	0.19	0.39		0.21	0.22	0.40
CaO	0.45	22.43		0.06	0.12	22.03	0.02	0.10	0.16	0.28	20.23	19.74	0.02	0.04	0.07	0.31	0.05	0.01	0.04
Na_2O	0.14	0.62				0.54				0.03	0.89	0.70					0.06		
K_2O																			
F																			
Cl																			
Total	100.85	99.87	99.46	99.55	99.51	98.55	100.21	99.05	99.04	100.18	99.64	99.94	100.28	98.15	100.19	100.15	99.83	101.68	99.30
Cr/Cr+Al			70.62				44.27						42.35	73.49			73.44	43.69	
Mg/Mg+Fe	93.45	88.25	62.68	92.52	92.47	91.32	70.47	92.39	94.10	92.70	92.34	91.86	69.16	49.66	92.06	93.62	66.79	73.70	92.70

Table 2. cont.

Garnet-free Peridotites

	LB-6							LB-7				LB-8				LB-9			
	opx	cpx	cpx in vein	sp	ol matrix	ol patch	phlog	opx	cpx	sp	ol	opx	cpx in vein	sp	ol	opx	cpx in vein	sp	ol
SiO_2	57.63	53.74	52.18	0.36	41.19	41.51	38.10	57.09	53.53	0.08	40.89	57.71	51.95	0.06	41.04	57.15	53.43	0.05	40.84
TiO_2	0.00	0.16	0.71	0.20	0.00	0.01	4.18	0.18	0.80	1.88	0.02	0.01	1.55	0.30	0.00	0.00	1.02	0.31	0.01
V_2O_5				0.17						0.20				0.26				0.29	
Al_2O_3	1.29	2.01	2.58	13.26	0.01	0.04	14.86	1.53	1.17	15.88	0.02	0.54	1.66	13.37	0.01	0.50	0.67	11.88	0.02
Cr_2O_3	0.26	1.26	0.52	54.05	0.03	0.16		0.78	0.87	50.12	0.05	0.22	0.78	55.91	0.01	0.11	0.00	58.17	0.02
FeO	4.71	1.84	2.69	16.61	7.56	5.91	3.44	4.40	3.49	13.96	7.35	4.13	3.58	13.40	6.62	4.05	3.35	14.20	6.56
MnO	0.11	0.05	0.06	0.22	0.10	0.10	0.02	0.11	0.12	0.15	0.10	0.11	0.08	0.18	0.09	0.02	0.03	0.19	0.09
MgO	35.75	17.61	16.81	14.71	50.96	52.00	22.65	34.55	17.83	17.23	50.75	36.73	17.00	16.26	51.10	35.80	17.54	15.47	51.04
NiO				0.16	0.36	0.37				0.16	0.36			0.19	0.39			0.15	0.37
CaO	0.37	22.71	23.23	0.02	0.03	0.19	0.06	1.23	20.75	0.00	0.07	0.27	21.46	0.02	0.04	0.18	22.31	0.00	0.04
Na_2O	0.10	0.59	0.51				1.46	0.21	0.72			0.03	0.68			0.02	0.62		
K_2O							8.46												
F							2.57												
Cl							0.00												
Total	100.22	99.97	99.29	99.79	100.24	100.29	100.00	100.08	99.28	99.68	99.61	99.75	98.74	99.96	99.30	97.83	98.97	100.75	98.99
Cr/Cr+Al				73.22						67.92				73.72				76.66	
Mg/Mg+Fe	93.11	94.46	91.76	61.22	92.32	94.01	92.14	93.33	90.11	68.75	92.49	94.06	89.44	68.39	93.23	94.03	90.32	66.01	93.28

	LB-14			LB-16			LB17								
	opx	cpx 2ndry?	ol	opx	cpx	ol	opx	opx vein	cpx in vein	sp	ol matrix	ol vein	phlog	rutile	
SiO_2	57.78	54.43	40.98	56.84	54.13	40.34	57.37	56.96	52.13	0.08	40.52	40.30	39.16	0.25	
TiO_2	0.06	0.44	0.01	0.16	0.66	0.01	0.11	0.24	1.44	1.97	0.00	0.03	7.89	83.71	
V_2O_5										0.22				0.84	
Al_2O_3	0.57	1.93	0.01	1.42	1.55	0.01	0.70	0.33	1.97	12.56	0.00	0.00	12.17	0.04	
Cr_2O_3	0.23	2.16	0.01	0.63	1.58	0.03	0.27	0.07	0.49	50.82	0.03	0.05		1.71	
FeO	4.15	2.17	6.88	4.97	3.10	7.97	5.32	6.68	4.13	19.17	8.16	9.43	5.90	5.19	
MnO	0.09	0.06	0.10	0.11	0.10	0.11	0.61	0.15	0.12	0.19	0.10	0.12	0.06	0.05	
MgO	36.25	16.92	50.84	34.94	19.09	50.51	35.38	34.69	17.30	14.76	50.25	49.23	19.89	2.15	
NiO			0.35			0.38				0.14	0.34	0.35		0.04	
CaO	0.42	19.35	0.03	0.67	18.50	0.03	0.57	0.68	21.13	0.02	0.06	0.07	0.24	0.04	
Na_2O	0.09	1.97		0.17	1.17		0.10	0.09	0.62				0.49		
K_2O													9.44		
F													2.89		
Cl													0.01		
Total	99.64	99.43	99.21	99.91	99.88	99.39	100.43	99.89	99.33	99.98	99.46	99.58	100.00	94.03	
Cr/Cr+Al										73.08					
Mg/Mg+Fe	93.96	93.29	92.95	92.61	91.65	91.87	92.22	90.25	88.19	57.85	91.65	90.30	85.74		

Table 2. cont.

Garnet-free Peridotites

	LB-18						LB-19-R					LB-21				LB-22			
	opx	cpx sp rim	sp	ol	phlog	rutile	opx	cpx	sp	ol	phlog	cpx	sp	ol	Prvskte	opx	cpx	sp	ol
SiO_2	57.07	53.53	0.08	41.22	38.21	0.03	56.49	53.59	0.06	40.51	39.21	54.80	0.12	40.55	0.11	57.11	53.23	0.06	40.99
TiO_2	0.17	0.51	3.44	0.03	5.27	95.90	0.05	0.21	0.50	0.01	1.12	0.53	2.61	0.00	56.25	0.03	0.53	0.83	0.01
V_2O_3			0.20			0.84			0.27				0.25		0.48			0.20	
Al_2O_3	1.53	1.13	11.95	0.02	15.32	0.05	1.85	2.14	15.09	0.02	14.79	0.71	2.63	0.00	0.09	1.57	2.21	17.97	0.01
Cr_2O_3	0.77	1.57	50.21	0.06		1.67	0.31	1.78	43.15	0.02		1.81	61.27	0.01	0.00	0.32	0.96	47.92	0.01
FeO	4.43	2.42	17.58	7.42	3.74	0.46	5.56	2.50	14.45	8.99	3.10	2.13	18.41	6.91	1.24	4.67	2.97	16.68	7.60
MnO	0.09	0.06	0.19	0.13	0.03	0.00	0.12	0.08	0.18	0.12	0.03	0.06	0.22	0.10	0.00	0.10	0.10	0.17	0.12
MgO	35.04	18.61	15.31	50.93	21.86	0.10	34.55	17.26	15.62	49.58	23.48	17.69	13.24	50.87	0.07	35.35	18.76	15.65	49.94
NiO			0.19	0.39		0.00			0.09	0.36			0.15	0.40	0.03			0.16	0.36
CaO	0.69	20.76	0.00	0.05	0.03	0.00	0.80	21.36	0.00	0.06	0.02	20.45	0.06	0.04	37.55	0.36	19.78	0.03	0.04
Na_2O	0.28	0.69			0.46	0.00	0.11	0.97			0.84	1.50				0.10	0.72		
K_2O					9.97						4.54								
F					0.73						0.90								
Cl					0.01						0.02								
Total	100.07	99.28	99.16	100.25	100.00	99.05	99.84	99.89	89.44	99.67	100.00	99.68	99.00	98.88	95.93	99.61	99.26	99.71	99.08
Cr/Cr+Al			73.81						65.73				93.99					64.14	
Mg/Mg+Fe	93.37	93.20	60.83	92.45	91.25		91.72	92.49	65.84	90.77	93.10	93.67	56.18	92.92	92.92	93.10	91.84	62.59	92.14

	LB-23						LB-25						LB-26				
	opx	cpx in vein	sp in vein	ol	phlog	rutile	opx	cpx in vein	sp	ol	ol matrix	phlog in vein		opx	cpx	sp 2ndry?	ol	
SiO_2	56.77	53.58	0.08	40.66	38.14	0.08		57.32	53.41	0.03	41.03	41.13	39.18		57.42	53.59	0.08	40.25
TiO_2	0.00	0.29	0.81	0.00	4.85	94.70		0.11	0.50	1.08	0.00	0.00	3.47		0.14	1.01	3.59	0.02
V_2O_3			0.22			0.94				0.28							0.26	
Al_2O_3	1.49	2.12	14.82	0.01	14.41	0.05		0.72	1.54	10.61	0.00	0.01	13.62		0.84	1.13	10.35	0.01
Cr_2O_3	0.29	1.08	51.42	0.02		2.96		0.34	1.35	55.71	0.03	0.17			0.33	1.34	52.67	0.04
FeO	4.41	2.59	16.70	7.15	3.22	0.25		4.92	2.37	16.45	8.05	6.88	3.29		4.63	2.79	16.81	7.76
MnO	0.08	0.06	0.24	0.10	0.02	0.00		0.13	0.08	0.21	0.14	0.12	0.01		0.12	0.08	0.21	0.12
MgO	35.54	18.50	14.27	50.84	21.87	0.02		35.36	17.82	14.44	50.05	51.07	23.16		35.52	17.12	14.86	49.90
NiO			0.14	0.38		0.00				0.14	0.37	0.31					0.20	0.38
CaO	0.43	20.24	0.06	0.05	0.02	0.02		0.63	21.53	0.03	0.04	0.17	0.00		0.53	21.38	0.01	0.06
Na_2O	0.09	0.76			0.87			0.11	0.80				0.58		0.13	1.04		
K_2O					9.33								9.91					
F					1.09								1.16					
Cl					0.00								0.00					
Total	99.10	99.22	98.78	99.21	100.00	99.03		99.64	99.40	99.01	99.71	99.86	100.00		99.66	99.48	99.06	98.54
Cr/Cr+Al			69.95							77.89							77.34	
Mg/Mg+Fe	93.49	92.72	60.37	92.69	92.37			92.76	93.06	61.01	91.73	92.97	92.62		93.18	91.62	61.18	91.98

Table 2. cont.

Garnet-free Peridotite																			
	LB-32						LB-33							LB-36					
	opx	cpx	sp	ol matrix	ol in vein	phlog	opx	cpx core	cpx rim	sp	ol	phlog	rutile	opx	cpx	sp	ol		
SiO_2	57.19	52.66	0.12	40.98	41.00	38.58	57.59	53.86	52.63	0.03	40.94	39.41	0.10	57.45	51.47	0.03	41.31		
TiO_2	0.08	1.40	1.75	0.02	0.02	5.90	0.24	0.87	1.22	3.46	0.01	5.15	70.18	0.00	0.53	0.02	0.01		
V_2O_5			0.20							0.28			0.79			0.13			
Al_2O_3	1.49	2.31	21.41	0.02	0.03	14.06	0.65	1.83	1.97	8.69	0.00	13.60	1.27	1.71	3.88	32.84	0.01		
Cr_2O_3	0.36	0.35	45.10	0.06	0.09		0.24	1.04	2.00	53.56	0.02		10.12	0.24	2.02	34.82	0.00		
FeO	4.31	2.75	14.19	7.25	5.10	3.27	5.07	2.66	2.52	17.52	8.21	2.92	4.80	4.98	2.72	15.59	7.35		
MnO	0.12	0.11	0.19	0.09	0.08	0.02	0.11	0.08	0.08	0.20	0.11	0.02	0.00	0.12	0.07	0.17	0.13		
MgO	35.88	17.60	17.28	51.32	52.80	21.94	35.32	17.55	16.79	15.60	50.17	22.84	6.08	35.86	16.63	16.87	51.16		
NiO			0.19	0.36	0.29					0.21	0.30		0.02			0.18	0.41		
CaO	0.37	21.74	0.01	0.06	0.17	0.01	0.73	19.81	20.48	0.01	0.05	0.02	3.94	0.22	21.24	0.01	0.02		
Na_2O	0.10	0.58				0.44	0.09	1.52	1.10			0.72		0.02	1.06				
K_2O						10.04						9.73							
F						0.82						0.71							
Cl						0.01						0.01							
Total	99.90	99.50	100.52	100.16	99.58	100.00	100.04	99.22	98.79	99.60	99.81	100.00	97.32	100.60	99.62	100.77	100.40		
Cr/Cr+Al			58.56							80.52						41.56			
Mg/Mg+Fe	93.68	91.94	68.47	92.66	94.86	92.29	92.54	92.16	92.24	61.35	91.59	93.31		92.77	91.60	65.86	92.54		
	LB-39						LB-40						LB-54						
	opx	cpx	sp	ol matrix	ol patch		opx	sp	ol	opx	cpx core	cpx rim	cpx patch	sp	ol matrix	ol patch			
SiO_2	57.58	53.06	0.04	41.17	41.24		56.58	0.08	41.17	56.80	53.75	52.83	51.05	0.06	40.89	41.23			
TiO_2	0.00	0.39	0.53	0.01	0.01		0.06	0.99	0.01	0.10	0.42	0.70	1.99	1.29	0.01	0.01			
V_2O_5			0.19					0.23						0.28					
Al_2O_3	0.94	2.82	16.38	0.01	0.02		1.92	16.68	0.01	1.71	2.97	2.52	3.49	19.53	0.02	0.03			
Cr_2O_3	0.21	2.07	51.90	0.04	0.09		0.72	50.10	0.01	0.35	1.10	0.87	0.37	46.35	0.02	0.11			
FeO	4.85	2.61	14.55	7.70	7.01		4.74	14.63	7.49	5.41	2.71	3.69	3.51	17.37	8.73	7.53			
MnO	0.09	0.08	0.15	0.12	0.11		0.10	0.19	0.11	0.11	0.08	0.11	0.10	0.22	0.11	0.10			
MgO	36.18	18.54	16.47	50.81	51.03		35.00	15.79	51.07	34.82	17.98	18.37	16.96	14.70	49.98	50.49			
NiO			0.18	0.41	0.41			0.21	0.40					0.15	0.39	0.39			
CaO	0.29	19.65	0.02	0.08	0.12		0.69	0.01	0.05	0.58	19.11	19.40	21.73	0.03	0.07	0.14			
Na_2O	0.08	0.71					0.13			0.11	1.39	0.75	0.40						
K_2O																			
F																			
Cl																			
Total	100.22	99.93	100.43	100.35	100.04		99.94	98.93	100.32	99.99	99.51	99.24	99.60	100.02	100.22	100.03			
Cr/Cr+Al			68.01					66.83						61.42					
Mg/Mg+Fe	93.00	92.68	66.87	92.17	92.85		92.94	65.80	92.40	91.98	92.21	89.87	89.60	60.14	91.08	92.28			

Table 2. cont.

Garnet-free Peridotites

LB-55

	opx	cpx lathe	sp	ol matrix	ol patch
SiO_2	57.21	53.69	0.72	41.04	41.31
TiO_2	0.00	0.10	0.10	0.01	0.02
V_2O_5			0.24		
Al_2O_3	1.40	2.16	17.61	0.00	0.00
Cr_2O_3	0.28	0.60	48.94	0.00	0.02
FeO	4.64	2.74	16.59	7.11	7.05
MnO	0.12	0.07	0.23	0.11	0.09
MgO	35.94	17.25	15.16	51.06	51.11
NiO			0.16	0.41	0.41
CaO	0.20	22.25	0.15	0.01	0.02
Na_2O	0.05	0.71			
K_2O					
F					
Cl					
Total	99.84	99.57	99.94	99.75	100.03
Cr/Cr+Al			65.09		
Mg/Mg+Fe	93.24	91.82	61.97	92.76	92.82

LB-60

	opx core	opx rim	cpx	cpx 2ndry	sp core	sp rim	ol	phlog
SiO_2	57.35	56.41	52.95	53.39	0.04	0.05	40.99	38.20
TiO_2	0.14	0.25	0.96	1.15	2.36	2.55	0.02	4.70
V_2O_5					0.21	0.23		
Al_2O_3	0.73	1.45	4.08	0.85	12.66	13.42	0.01	15.03
Cr_2O_3	0.24	0.71	2.90	0.71	52.36	51.69	0.05	
FeO	4.40	4.55	2.52	2.93	15.21	14.69	7.22	3.27
MnO	0.10	0.10	0.06	0.11	0.13	0.13	0.12	0.03
MgO	35.82	34.81	16.11	18.81	16.53	16.99	50.38	21.44
NiO					0.21	0.26	0.38	
CaO	0.51	0.81	16.78	20.27	0.01	0.01	0.07	0.00
Na_2O	0.14	0.22	2.81	0.48				0.43
K_2O								10.15
F								0.89
Cl								0.01
Total	99.43	99.31	99.17	98.70	99.74	100.04	99.24	100.00
Cr/Cr+Al					73.51	72.10		
Mg/Mg+Fe	93.55	93.16	91.93	91.97	65.96	67.34	92.56	92.12

LB-61

	opx	cpx in vein	sp	sp 2ndry	ol matrix	ol patch	phlog
SiO_2	56.64	52.49	0.07	0.11	41.37	41.44	37.90
TiO_2	0.10	1.74	0.66	1.08	0.01	0.03	7.37
V_2O_5			0.23	0.20			
Al_2O_3	2.20	1.08	17.74	19.94	0.03	0.05	12.95
Cr_2O_3	0.69	0.63	50.14	48.59	0.06	0.13	
FeO	4.57	3.54	14.74	13.32	7.38	5.66	6.77
MnO	0.12	0.12	0.18	0.19	0.14	0.09	0.04
MgO	34.95	17.54	16.46	17.08	50.89	51.76	20.03
NiO			0.15	0.16	0.42	0.32	
CaO	0.56	21.95	0.01	0.03	0.04	0.03	0.02
Na_2O	0.21	0.51					0.81
K_2O							8.93
F							1.35
Cl							0.00
Total	100.04	99.60	100.42	100.71	100.34	99.51	100.00
Cr/Cr+Al			65.47	62.05			
Mg/Mg+Fe	93.16	89.83	66.57	69.57	92.48	94.22	84.06

Spinel-facies Peridotites

LB-11

	opx	cpx 2ndry	cpx high Ca	sp	ol
SiO_2	56.03	53.39	52.77	0.06	40.77
TiO_2	0.07	0.35	0.28	0.53	0.02
V_2O_5				0.17	
Al_2O_3	2.78	3.37	3.22	30.15	0.02
Cr_2O_3	0.64	1.49	1.76	36.54	0.02
FeO	4.74	2.29	2.88	14.21	7.49
MnO	0.10	0.08	0.08	0.09	0.12
MgO	34.70	16.40	19.82	17.52	50.46
NiO				0.14	0.39
CaO	0.63	20.30	17.85	0.00	0.04
Na_2O	0.10	1.67	0.62		
K_2O					
F					
Cl					
Total	99.79	99.34	99.28	99.45	99.33
Cr/Cr+Al				44.84	
Mg/Mg+Fe	92.88	92.74	92.46	68.73	92.31

LB-29

	opx	sp	ol
SiO_2	56.55	0.04	40.55
TiO_2	0.08	0.24	0.00
V_2O_5		0.09	
Al_2O_3	2.59	31.58	0.03
Cr_2O_3	0.55	36.75	0.03
FeO	4.71	12.86	7.35
MnO	0.13	0.05	0.12
MgO	34.94	18.02	50.56
NiO		0.16	0.38
CaO	0.63	0.00	0.05
Na_2O	0.17		
K_2O			
F			
Cl			
Total	100.35	99.82	99.07
Cr/Cr+Al		43.84	
Mg/Mg+Fe	92.97	71.41	92.46

LB-31

	opx	cpx	sp	ol
SiO_2	55.91	53.53	2.16	40.62
TiO_2	0.06	0.15	0.35	0.00
V_2O_5			0.16	
Al_2O_3	3.19	3.68	30.10	0.01
Cr_2O_3	0.81	1.27	34.56	0.01
FeO	4.97	2.23	12.66	7.71
MnO	0.12	0.08	0.04	0.10
MgO	34.26	16.69	18.69	50.33
NiO			0.19	0.40
CaO	0.83	21.11	0.01	0.04
Na_2O	0.09	1.29		
K_2O				
F				
Cl				
Total	100.24	100.03	98.96	99.22
Cr/Cr+Al			43.51	
Mg/Mg+Fe	92.47	93.03	72.47	92.09

Table 2. cont.

	Fe-rich dunites and wehrlites																
	KAT 5		KAT 7	KAT 10			KAT 12			KAT 14			LB-15			LB-59	
	sp	ol	ol	opx	cpx	ol	cpx	ol	cpx	sp	ol	cpx	sp	ol	ol	phlog
SiO_2	0.44	39.97	40.01	56.23	51.06	39.49	53.23	39.86	53.40	0.11	39.67	54.36	0.13	39.77	39.42	36.67
TiO_2	6.17	0.02	0.03	0.31	1.89	0.04	0.37	0.01	0.51	5.41	0.03	0.43	1.53	0.00	0.03	3.75
V_2O_5	0.31									0.23			0.26			
Al_2O_3	7.52	0.01	0.03	1.60	1.88	0.01	1.24	0.03	0.96	11.96	0.02	1.86	8.51	0.02	0.04	15.81
Cr_2O_3	36.15	0.03	0.04	0.22	0.63	0.01	1.05	0.02	1.59	39.41	0.03	0.29	52.38	0.03	0.01	
FeO	33.81	12.93	13.21	8.03	4.97	13.44	3.85	13.39	3.75	29.61	12.70	4.36	21.19	13.18	14.29	6.04
MnO	0.26	0.16	0.15	0.15	0.08	0.14	0.08	0.16	0.09	0.21	0.16	0.12	0.38	0.18	0.16	0.02
MgO	11.45	46.23	46.47	32.17	16.01	46.22	16.79	45.59	17.28	12.25	46.50	17.13	11.01	46.63	45.91	20.67
NiO	0.29	0.31	0.33			0.33		0.27		0.24	0.33		0.21	0.35	0.27	
CaO	0.04	0.07	0.07	0.86	22.10	0.07	20.56	0.06	20.76	0.00	0.07	19.93	0.13	0.04	0.09	0.01
Na_2O				0.27	0.72		0.79		0.91			1.43				0.28
K_2O															10.30	
F																0.55
Cl																0.00
Total	96.46	99.71	100.33	99.84	99.34	99.75	97.96	99.39	99.25	99.46	99.51	99.91	95.81	100.20	100.22	100.00
Cr/Cr+Al	76.33									68.85			80.50			
Mg/Mg+Fe	37.65	86.44	86.25	87.71	85.17	85.98	88.60	85.86	89.15	42.45	86.72	87.51	48.09	86.32	85.14	85.92

	Fe-rich dunites and wehrlites																	Glimmerite	
	LB-19-C			LB-46				LB-51					LB-58					LB49	
	sp	ol	phlog	opx	cpx core	cpx rim	ol	cpx	sp corecpx	sp inclsn	ol		cpx	sp	ol matrix	ol patch	phlog	phlog	ilmnte
SiO_2	0.06	39.98	39.06	56.08	52.55	52.89	39.82	53.64	0.13	2.43	39.90		51.35	0.03	39.93	40.10	39.81	39.28	0.02
TiO_2	5.26	0.04	3.63	0.28	0.86	1.12	0.03	0.50	5.87	4.61	0.04		1.37	1.08	0.00	0.01	5.81	3.78	49.19
V_2O_5	0.34								0.30	0.35				0.25					0.37
Al_2O_3	7.48	0.02	13.63	1.56	1.61	3.78	0.06	1.20	9.80	6.83	0.04		2.04	16.10	0.01	0.02	11.18	12.86	0.12
Cr_2O_3	48.10	0.04		0.45	1.86	1.46	0.05	1.65	40.67	39.14	0.01		0.55	45.66	0.03	0.14			1.66
FeO	22.50	12.33	4.74	7.12	3.50	4.25	12.18	3.85	29.13	35.67	12.69		4.09	23.18	10.49	9.93	4.72	6.65	32.95
MnO	0.24	0.16	0.04	0.14	0.10	0.08	0.16	0.09	0.21	0.41	0.15		0.04	0.23	0.16	0.12	0.02	0.04	0.29
MgO	12.31	47.30	22.11	33.12	17.54	16.88	47.68	18.15	12.61	7.26	46.99		15.69	12.87	48.08	48.60	22.24	21.90	11.31
NiO	0.19	0.33					0.32		0.26	0.19	0.29			0.19	0.36	0.37			0.13
CaO	0.01	0.07	0.02	0.80	19.63	15.92	0.07	19.53	0.00	0.18	0.07		23.22	0.00	0.06	0.15	0.06	0.00	0.21
Na_2O			0.62	0.26	0.99	2.48		0.98					0.53				0.34	0.55	
K_2O			9.59														10.01	10.05	
F			0.59														3.93	0.48	
Cl			0.02														0.01	0.00	
Total	96.52	100.27	100.00	99.81	98.64	98.86	100.37	99.59	98.98	97.08	100.18		98.88	99.63	99.12	99.44	100.00	100.00	96.25
Cr/Cr+Al	81.18								73.57	79.36				65.55					
Mg/Mg+Fe	49.38	87.24	89.27	89.23	89.93	87.63	87.47	89.37	43.56	26.63	86.85		87.24	49.75	89.10	89.72	89.36	85.45	

as iron oxide, rutile, zircon, nepheline, perovskite, calcium carbonate, and harmatome are observed in a few samples (Table 1). They tend to associate with specific metasomatic mineral assemblages, whose petrography is described elsewhere (Chesley *et al.*, 1998; Dawson, this volume; Lee and Rudnick, 1998 and unpublished data; Rudnick *et al.*, this volume).

5. MINERAL CHEMISTRY

Mineral analyses were performed at Harvard on a Camebax MBX electron microprobe in wavelength dispersive mode using 15 kV and a 15 nA beam current. Whole-rock major elements were determined by X-ray fluorescence at the University of Massachusetts, Amherst, on a Siemens MRS 400 MP simultaneous spectrometer.

5.1 Olivine

Olivines are unzoned and have forsterite contents ranging from 85.1 to 93.3, NiO ranging from 0.27 to 0.42 wt. %, and Cr_2O_3 ranging from 0 to 0.10 wt. %. Compositions are generally homogeneous within a given sample. Exceptions are composite or veined specimens, in which olivine compositions grade with distance from veins (LB17, 19), and olivine inclusions within former garnet, which can be more forsteritic than groundmass olivines (e.g. $Fo_{92.4}$ in garnet and $Fo_{89.9}$ in groundmass of LB34). Similar forsteritic olivine inclusions have been observed in garnet xenocrysts in Colorado Plateau kimberlites and attributed to partial reequilibration during cooling (Smith and Wilson, 1985). However, the Tanzanian specimens have high equilibration temperatures and are likely to have been heated (discussed later). Thus the olivine inclusion probably represents an original groundmass composition, which has remained shielded from chemical change by the surrounding garnet. Rudnick *et al.* (1994) reported similar forsteritic olivine inclusions in garnet from Lashaine peridotites.

In a few samples, late-stage olivine occurs as tiny euhedral grains associated with patches of clinopyroxene and chromite intergrowths or in metasomatic veins and patches. These olivines are generally more Mg-rich than the groundmass olivines. In LB 6, for example, the groundmass olivine is $Fo_{92.3}$ while the euhedral grains are $Fo_{94.0}$. In these tiny euhedral olivines NiO is anomalously low, as evinced by lower NiO/MgO (<0.0070), compared to primary olivines (NiO/MgO = 0.0076 ± 0.00035).

5.2 Orthopyroxene

Orthopyroxenes are mostly unzoned, but in a few samples they are slightly enriched in CaO (>1.0 %) on the rims, suggesting heating. Cr_2O_3 ranges from 0.21 to 0.81 wt. % and correlates roughly with Al_2O_3 (Table 2). CaO ranges from near detection limit to 1.8 wt. % and exhibits a rough negative correlation with Mg# (100 Mg/Mg+Fe) and positive correlation with Al_2O_3 (Fig. 3a, b). Most of the orthopyroxenes have Al_2O_3 < 2.0 wt.%, which is within the range observed for orthopyroxenes in Kaapvaal low temperature garnet peridotites, but distinct from those in spinel peridotites from alkali basalts (Boyd, 1989b). Low Al_2O_3 orthopyroxene is indicative of high pressure subsolidus assemblages (Yamada and Takahashi, 1984), and these rocks probably equilibrated at pressures greater than 30 kbar, within the garnet-facies, even though the samples do not contain garnet. The three samples that have high Al-orthopyroxene also contain hercynitic spinel and are interpreted as the only true spinel-facies peridotites in our collection (Table 2). Mg# of orthopyroxene correlates well with Fo in olivine, as expected in an equilibrium assemblage (Fig. 3b).

Orthopyroxenes in garnet kelyphites and coronas have higher CaO and Al_2O_3, and lower Mg# than primary orthopyroxenes. In LB4, corona orthopyroxenes have Al_2O_3 of 11.54 wt.%. Except for these, secondary orthopyroxenes are rare but occur occasionally in metasomatic veins. In LB17, for example, secondary orthopyroxene is associated with zircon, phlogopite, rutile, and sulfide, and is more Fe-rich than the primary orthopyroxene.

5.3 Clinopyroxene

Clinopyroxene in Labait xenoliths is compositionally variable (Table 2). In most samples, clinopyroxene appears to be secondary, based on its small grain size and on its tendency to be found between mineral grains, rimming other minerals such as chromite and orthopyroxene, or forming aggregate patches. Medium-sized clinopyroxene grains concentrated in metasomatic veins, dikes, or patches are typically cloudy and have higher CaO than the small secondary ones. Only in garnet-bearing samples are large primary clinopyroxene grains observed. These have lower CaO (<20 wt. %) than secondary clinopyroxenes (>20 wt. %) and generally have turbid rims, which sometimes differ in composition from the cores. For example, in LB 45, a garnet lherzolite, the cores of the clinopyroxenes have lower CaO (by ~2 wt. %) than the turbid rims. Zoning of other elements is also prevalent; in some samples, Mg# and Na_2O are lower on the rims, consistent with the results of Dawson *et al.* (1996). They also noted that Al_2O_3 is generally lower on the rims, but this is not always true in our samples.

When Mg# of clinopyroxene is plotted against Fo in olivine for all samples there is a considerable amount of scatter, unlike the tight correlation seen for orthopyroxene (Fig. 3b). Texturally secondary clinopyroxenes have lower Mg# than Fo of coexisting olivines, which is opposite to what is expected for an equilibrium assemblage. In contrast, large clinopyroxene grains in the matrix generally have Mg#'s that are the same or slightly higher than that of coexisting olivines.

5.4 Garnet

Garnet or its breakdown products are present in 8 of our samples, and in an additional six, reported by Dawson *et al.* (1996). All garnets are pyropic, with CaO between 3.72 to 6.73 wt. % and Cr_2O_3 from 3.46 to 7.34 wt. % (Fig. 3c); these garnets fall within the field of garnets from Kaapvaal garnet lherzolites. We have not observed subcalcic garnet compositions at Labait (CaO <4.0 wt. %), as is present at Lashaine (Pike *et al.*, 1980; Rudnick *et al.*, 1994).

Compositions of fine-grained inner kelyphite assemblages estimated by rastered probe analyses indicate slight loss of CaO and TiO_2 and gain of Na_2O, but are otherwise very similar to fresh garnet (e.g. LB12, 53) (Fig. 2b). The garnet cores thus appear to have undergone near isochemical decomposition. Formation of the outer corona assemblage undoubtedly involved heating and chemical exchange (e.g. Fe-enrichment (LB34), and sulfide and phlogopite addition (LB12)). Temperatures calculated using the Ca-in-orthopyroxene coexisting with clinopyroxene barometer (Brey and Köhler, 1990) indicate that the corona assemblages formed at higher temperatures. For example, in LB45 the symplectic orthopyroxene yields a temperature of 1474 °C while the groundmass orthopyroxene yields a temperature of 1382 °C (using the same thermometer). We thus infer that transient heating aided in the decomposition of garnet to form the outer corona. The fine-grained kelyphitic core is likely to be a result of decompression during entrainment by the erupting lava because of the aphyric texture and isochemical nature of the decomposition; the texture suggests that the process was rapid.

Table 3. Whole-rock Major Element Chemistry.

	SiO_2	TiO_2	Al_2O_3	FeO(t)	MnO	MgO	CaO	Na_2O	K_2O	P_2O_5	Total	Mg#
Garnet Lherzolites												
LB 12	43.64	0.05	1.98	8.34	0.15	42.10	1.79	0.02	0.05	0.02	98.13	90.00
LB-45	43.28	0.20	3.89	8.34	0.15	38.67	2.74	0.11	0.08	0.02	97.48	89.21
Garnet Harzburgites												
LB 2	43.49	0.06	1.18	6.59	0.13	45.94	0.50	0.00	0.12	0.02	98.02	92.55
LB 4	44.64	0.03	1.54	7.55	0.14	43.30	1.06	0.00	0.03	0.01	98.30	91.09
LB 24	43.21	0.06	1.21	6.92	0.12	45.68	0.61	0.00	0.05	0.01	97.87	92.17
LB-34	41.09	0.17	0.68	9.28	0.14	45.78	0.43	0.00	0.09	0.01	97.69	89.79
LB-50-1*	43.75	0.05	1.37	7.79	0.14	44.16	0.98	0.00	0.03	0.01	98.28	91.00
LB-50-2*	43.76	0.05	1.32	7.72	0.14	44.07	0.95	0.00	0.02	0.01	98.04	91.05
LB-53	42.57	0.12	1.73	7.93	0.14	43.89	1.34	0.00	0.04	0.01	97.75	90.80
KAT 17	44.80	0.06	0.41	10.55	0.13	43.28	0.64	0.09	0.02	0.02	100.00	87.97
GL4201†	42.67	0.12	1.06	9.10	0.13	44.87	1.15	0.16	0.06	0.01	99.33	89.79
GL4202†	44.07	0.03	1.21	7.91	0.12	44.62	1.01	0.05	0.06	0.01	99.09	90.96
GL4203†	43.71	0.02	1.12	7.93	0.12	44.98	0.96	0.01	0.06	0.01	98.92	91.00
GL4206†	44.39	0.03	1.30	7.86	0.13	44.20	0.85	0.02	0.06	0.02	98.86	90.94
Garnet-free Peridotites												
KAT 1	45.54	0.106	0.65	7.04	0.109	45.97	0.39	0.07	0.09	0.042	100.01	92.09
LB 1	43.83	0.08	0.40	6.38	0.12	47.34	0.25	0.00	0.04	0.02	98.45	92.98
LB 6	41.43	0.12	0.65	7.38	0.13	47.67	0.56	0.00	0.15	0.04	98.13	92.01
LB 7	40.84	0.11	0.55	7.50	0.13	47.98	0.28	0.00	0.13	0.02	97.53	91.94
LB 8	42.83	0.05	0.34	6.40	0.11	47.38	0.18	0.00	0.05	0.01	97.36	92.96
LB 9	41.97	0.06	0.36	6.50	0.12	47.45	0.22	0.00	0.05	0.02	96.74	92.86
LB 14	41.28	0.08	0.33	7.15	0.12	48.88	0.04	0.00	0.07	0.01	97.95	92.42
LB 16	42.89	0.12	0.60	7.21	0.13	46.29	0.40	0.00	0.07	0.03	97.74	91.96
LB 17	44.23	0.24	0.56	7.41	0.14	44.85	0.42	0.00	0.07	0.02	97.93	91.52
LB 18	41.57	0.10	0.42	8.31	0.13	47.15	0.38	0.00	0.06	0.01	98.13	91.01
LB 19-R	42.23	0.08	0.82	8.51	0.15	45.76	0.46	0.00	0.25	0.01	98.26	90.55
LB 21	40.75	0.09	0.30	6.52	0.12	48.85	0.52	0.00	0.08	0.03	97.26	93.04
LB 22	43.09	0.07	0.67	7.44	0.13	45.93	0.39	0.00	0.06	0.02	97.79	91.67
LB 23	42.48	0.03	0.54	7.22	0.13	47.34	0.41	0.00	0.06	0.03	98.24	92.12
LB 26	41.97	0.13	0.45	7.07	0.13	47.01	0.18	0.00	0.06	0.01	97.02	92.22
LB 32	43.51	0.09	0.60	6.61	0.12	46.77	0.26	0.00	0.10	0.03	98.07	92.66
LB-33	42.00	0.33	0.60	7.31	0.13	46.54	0.69	0.00	0.14	0.01	97.76	91.90
LB-36	43.56	0.06	0.88	6.95	0.13	45.36	0.61	0.00	0.13	0.03	97.71	92.09
LB-39	44.23	0.14	0.86	7.73	0.14	44.04	0.72	0.00	0.15	0.03	98.04	91.04
LB 40	43.23	0.05	0.52	7.03	0.13	47.02	0.23	0.00	0.03	0.00	98.24	92.26
LB-54	43.21	0.17	1.13	7.50	0.14	44.29	1.26	0.07	0.24	0.04	98.04	91.32
LB-55	43.00	0.08	0.76	6.79	0.13	46.12	0.41	0.00	0.22	0.02	97.53	92.37
LB-60	43.28	0.14	0.50	6.78	0.13	46.56	0.28	0.00	0.08	0.02	97.77	92.45
LB-61	42.24	0.09	0.50	7.00	0.13	47.68	0.23	0.00	0.09	0.02	97.98	92.40
Spinel-facies Peridotites												
LB 11	43.07	0.04	0.84	7.18	0.13	46.37	0.30	0.00	0.04	0.00	97.97	92.00
LB 29	42.89	0.06	0.88	7.10	0.13	46.52	0.30	0.00	0.06	0.01	97.96	92.11
LB-31	43.69	0.04	1.02	7.30	0.14	45.25	0.96	0.00	0.08	0.01	98.48	91.70
Cumulates												
LB 15	45.80	0.25	1.23	8.63	0.16	32.36	8.38	0.84	0.07	0.01	97.73	86.99
LB 19-C	39.54	0.25	0.84	12.88	0.18	43.15	0.21	0.00	0.50	0.01	97.53	85.66
LB 43	39.88	0.10	0.26	11.86	0.17	45.79	0.13	0.00	0.07	0.01	98.27	87.31
LB-46	40.69	0.22	0.51	11.22	0.16	43.21	1.56	0.00	0.06	0.01	97.65	87.29
LB-51	42.15	0.31	1.12	11.25	0.16	39.48	3.37	0.18	0.20	0.05	98.27	86.22
LB-58	39.71	0.10	0.52	10.50	0.18	45.05	0.83	0.00	0.09	0.01	97.00	88.44
LB-59	39.06	0.09	0.27	14.10	0.18	43.76	0.09	0.00	0.13	0.02	97.68	84.70
LB49	39.36	5.339	12.56	8.32	0.05	21.13	0.32	0.42	9.68	0.064	97.25	81.91

*LB 50-1 was leached with acetic acid and LB 50-2 was leached with both acetic and dilute hydrochloric acid. †from Dawson *et al.* (1996)

Garnets in LB2 appear to have incongruently melted to an assemblage consisting of clinopyroxene, orthopyroxene, spinel, glass, and occasionally olivine. Hunter and Taylor (1982) described similar symplectic assemblages and also explained their origin by incongruent melting. Primary orthopyroxenes in LB2 have Al- and Ca-rich rims, suggesting that this xenolith was heated.

5.5 Chromite/Spinel

Chromite or spinel occurs in nearly all samples (Table 2, Fig. 3d). Three deep red hercynitic spinels (LB 11, 29, 31) with low Cr# <50 (100 Cr/Cr+Al) are typical of those found in spinel peridotites in alkali basalts (Fig. 3d). Because these spinels coexist with aluminous orthopyroxenes, these xenoliths are presumed to represent the few true spinel-facies peridotites in our collection. Spinel in LB 36 also have low Cr# and are deep red in color, however the aluminum content of coexisting othopyroxenes is low. Spinels precipitated during garnet breakdown tend to have ultra-low Cr#'s. The remaining chromite/spinel in Labait samples are opaque and have high Cr# (>60), overlapping the compositional range for chromites in garnet peridotites from Kaapvaal. In some garnet-free harzburgites, two generations of chromite or spinel occur (Fig. 3d).

Chromites are absent in the garnet-bearing peridotites at Labait (which only have secondary low Cr# spinel). The high Cr content of spinels may depress the garnet-spinel transition (O'Neill, 1981). For Cr# of ~70, the garnet-spinel transition is depressed to approximately 3.6 GPa, which coincides approxi-

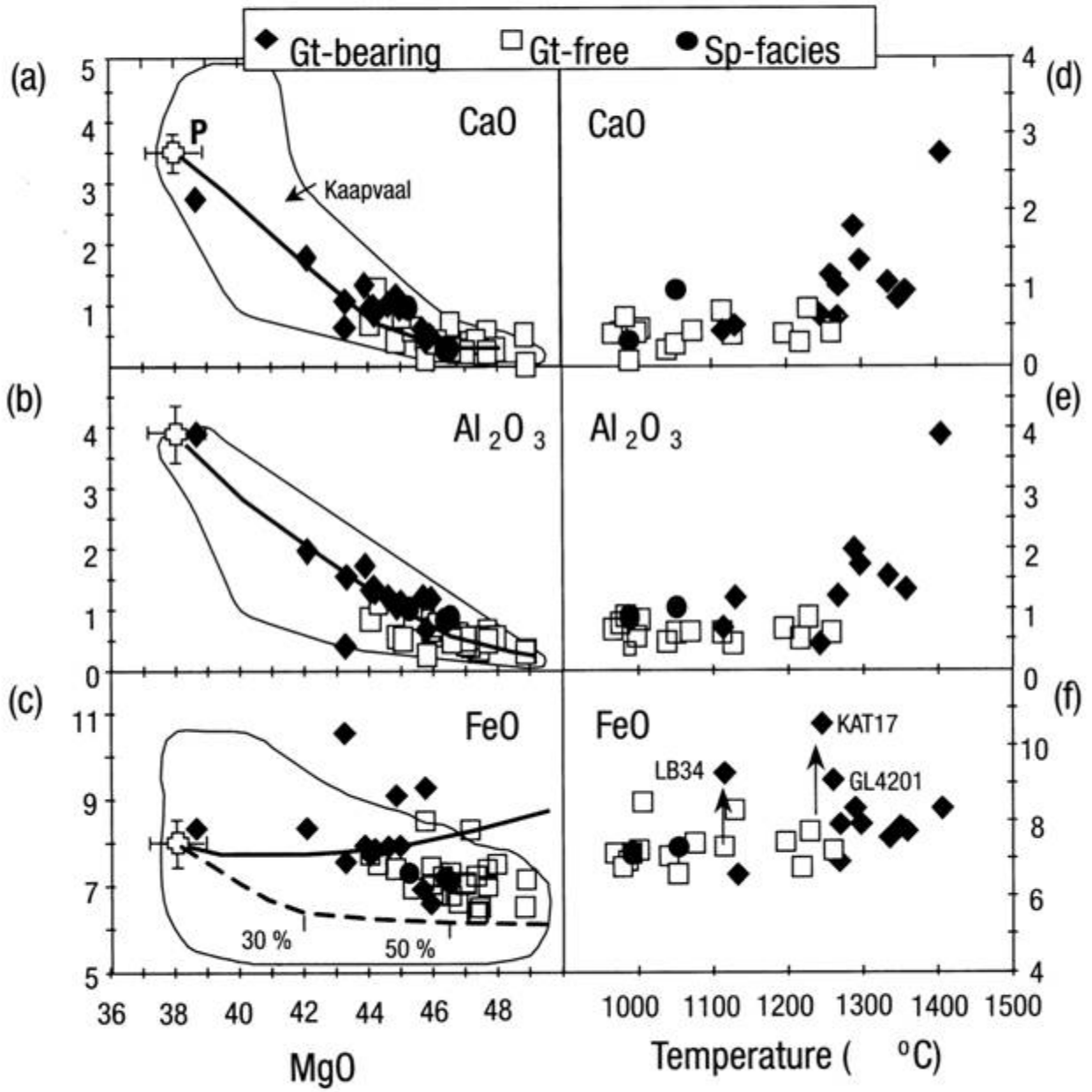

Figure 4. (a) (b) (c) Whole-rock CaO, Al_2O_3, and FeO (=FeO+Fe_2O_3) versus MgO, compared to Kaapvaal garnet peridotites. Partial melting curves for residues from Asimow (1998; solid lines) and Walter (1998b; dashed line). The former represent residues of polybaric batch melting calculated using MELTS and assuming a mantle potential temperature whose adiabat intersects the solidus at 2.5 GPa. The latter represents residues of isobaric batch melting at 7 GPa. Range of primitive mantle values taken from McDonough and Sun (1995) and Allegre *et al.* (1995). Note that three samples (KAT 17, LB34, and GL4201) show Fe-enrichment but no enrichment in CaO and Al_2O_3. **(d) (e) (f)** Whole-rock CaO, Al_2O_3, and FeO versus temperature. Temperatures calculated from two-pyroxene thermometer (Brey and Kohler, 1990). Arrows in **(f)** show direction of Fe-enrichment.

Table 4. Thermobarometry.

	T (Celsius) Garnet present	P (GPa)	T (Celsius) No Garnet	T (Celsius)	
	TBKN	PBKN	TBKN	T Ca-in-Opx	comments
Garnet Lherzolites					
LB-12	1290	4.4		1239	
LB-12*	1290	4.4			
LB-45*	1406	4.7		1382	
LB-45*				1462	gt breakdown
Garnet Harzburgites					
KAT-17	1245	4.0		923	
LB-2			1132 (3.5)	926	core
LB-2				1054	rim
LB-4*	1336	4.4		872	matrix
LB-4*				1302	gt breakdown
LB24	1265	4.4		1182	
LB-24*	1269	4.4		1190	
LB-34*	1115	3.7		1141	
LB-50*	1359	4.6		1313	
LB-53	1298	4.7		1257	
LB-53*	1297	4.7			
GL4201	1260	3.9		1186	
GL4201			1381 (4.5)	1539	gt breakdown
GL4202	1270	4.6		1332	
GL4202			1363 (4.5)	1407	gt breakdown
GL4203				1330	
GL4206	1350	4.9		1329	
GL4206			1330 (4.5)	1429	gt breakdown
GLX1	1290	4.6		1340	
GLX9	1240	4.3		1231	
Garnet-free Peridotites					
LB-14			990 (4.5)	993	
LB-16			1260 (4.5)	1100	
LB-17			1070 (4.5)	1074	
LB-18			1120 (4.5)	1107	
LB-22			1200 (4.5)	962	
LB-23			1000 (4.5)	999	
LB-26			1040 (4.5)	1044	
LB-32			1060 (4.5)	966	
LB-33			1110 (4.5)	1121	
LB-39			1230 (4.5)	919	
LB-54			1200 (4.5)	1065	
LB-55			980 (4.5)	854	
LB-60			1220 (4.5)	1036	core
LB-60				1150	rim
Spinel-Facies Peridotites					
LB-11			990 (2.5)	991	
LB-29			990 (2.5)	990	
LB-31			1050 (2.5)	1056	
Fe-rich dunite					
LB-46			1150 (4.5)	1149	

First two columns are for garnet-bearing samples.
Third column is T calculated for garnet-free samples; input P parenthesized.
Fourth column is temperatures calculated using Ca in orthopyroxene.
TBKN = two pyroxene thermometer of Brey and Kohler (1990).
PBKN = Al solubility in orthopyroxene coexisting with garnet barometer of Brey and Kohler (1990).
T Ca-in-Opx = CaO in orthopyroxene thermometer of Brey and Kohler (1990); input P = 4.5 GPa.
* Garnet composition using 800 V raster and 125 micrometer spot size to probe kelyphite.
Samples with GL-prefix are from Dawson *et al.* (1997).

mately with the equilibration pressure calculated for our shallowest garnet-bearing peridotite (3.7 GPa for LB 34).

5.6 Phlogopite

Phlogopite occurs in several samples as tiny lathes on grain boundaries, in veins, or in metasomatic patches of clinopyroxene and chromite (Table 2). Only in LB19, the composite xenolith, does phlogopite occur as large platy grains in textural equilibrium with the primary mineral assemblage. Phlogopite Mg# ranges from 84.0 to 93.3 for all samples. TiO_2 ranges from 3.63 to 7.89 wt. % except for LB19R (depleted portion of LB19) which has TiO_2 of 1.12 wt. %. Erlank *et al.* (1987) report that primary phlogopites from Kaapvaal garnet peridotites do not exceed 4.86 wt.% TiO_2, so most of the phlogopites reported here may be secondary.

We also analyzed the phlogopites which make up LB49, a glimmerite xenolith. These phlogopites have compositions within the range observed for the Labait phlogopites, suggesting a connection between the glimmerite and the phlogopites in Labait xenoliths.

Interestingly, two generations of phlogopite may occur within one xenolith. The texturally equilibrated phlogopites in LB19 exhibit compositional variation between the Fe-rich vein and depleted portions of the xenolith. The vein phlogopite has 3.63 wt. % TiO_2 and Mg# of 89.3, while the depleted portion has 1.12 wt. % TiO_2 and Mg# of 93.1. In LB34, phlogopites in garnet breakdown patches have higher Fe and Ti and lower Mg compared to those found as interstitial lathes in the primary groundmass.

6. MAJOR ELEMENT COMPOSITION

Whole-rock major-element compositions are presented in Table 3. For residual peridotites, Mg# is generally high (89 to 93 with most > 91) and similar to those of Kaapvaal peridotites (Mg# = 90-92; Boyd, 1989a). Garnet-bearing peridotites tend to have lower Mg# and Mg/Si than garnet-free peridotites. As

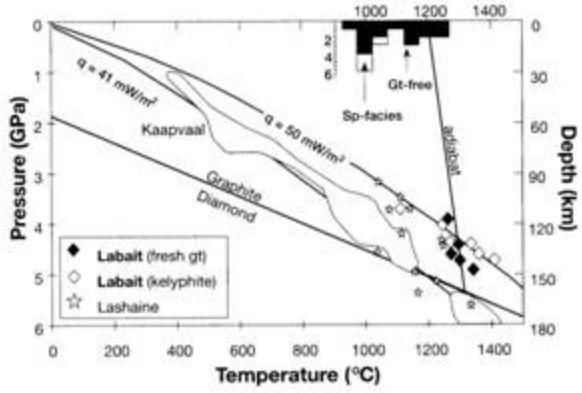

Figure 5. Pressure-temperature estimates of Labait garnet-bearing peridotites calculated from the Al-in-orthopyroxene barometer and two-pyroxene thermometer of Brey and Kohler (1990). Open diamonds represent P-T estimates determined by using the composition of fine-grained garnet kelyphites for those garnet-bearing peridotites in which fresh garnet is absent. Stars represent data from Lashaine garnet peridotites (Rudnick *et al.*, 1994; Rudnick *et al.*, unpublished). Histogram in upper left corner denotes temperature estimates for garnet-free peridotites (solid) and spinel peridotites (open). Geotherms taken from Rudnick *et al.* (1998), calculated assuming lithospheric mantle and crustal heat productions of 0.03 and 0.5 $\mu W/m^3$, respectively. Adiabatic temperature profile is for a 0.6°C/km gradient and a 1200°C potential temperature.

shown in Fig. 4a-c, Labait peridotites plot within the field of Kaapvaal garnet peridotites, but differ by having a more restricted range in compositions, which are highly refractory. The refractory character of Labait xenoliths is also reflected in the general absence of primary clinopyroxene and garnet. The spinel-facies peridotites (LB11, 29, 31) are highly refractory (Fig. 4a-c) in comparison to the average spinel peridotite reported by McDonough (1990) and more closely resemble spinel facies peridotites from Kaapvaal and Siberian cratons (Boyd, 1989a; Boyd *et al.*, 1997). Garnet-bearing peridotites are the most fertile of the residual peridotites in our collection, but are still considerably more refractory than the primitive mantle estimates. Only one sample (LB45) has a composition approaching primitive mantle.

In element-element plots, most xenoliths plot on coherent trends, which trend toward primitive mantle (Fig. 4a-c) and can therefore be explained as partial melting trends. However, some samples (KAT17, LB34, and GL4201, the latter from Dawson *et al.* (1996)) have higher FeO than primitive mantle (Fig. 4c), yet display refractory characteristics such as low CaO and Al_2O_3; these samples therefore plot off the trend in FeO-MgO space, but plot close to or on the trend in CaO and Al_2O_3 versus MgO space. One of these, LB 34, a garnet-bearing peridotite, has FeO of 9.28 wt. % (Mg# = 89.8) and contains a forsteritic olivine inclusion in a relict garnet (see previous sections) suggesting that this sample has been re-enriched in Fe. These observations suggest that local Fe-enrichment has been superimposed on the overall compositional trends exhibited by our xenoliths. As will be discussed below, the compositional trends correlate well with depth, so the few Fe-enriched samples represent minor perturbations to the compositional stratigraphy.

7. THERMAL STATE AND THICKNESS OF CRATONIC MANTLE

Pressures and temperatures of equilibration for garnet-bearing samples were calculated using the aluminum-in-orthopyroxene coexisting with garnet barometer (PBKN) and the two-pyroxene thermometer (TBKN) (Brey and Köhler, 1990) assuming no Fe^{3+} (Table 4, Fig. 5). Only four of our samples (KAT 17, LB 12, 24, 53) have relict garnet. Raster analyses on the fine-grained inner kelyphite assemblages were used to calculate P/T for those samples without relict garnet. The P/Ts calculated for fresh and altered garnet are indistiguishable to within error. For garnet-free samples, temperatures were calculated using TBKN and by assuming an input pressure of 4.5 GPa for most samples (2.5 GPa was assumed for spinel peridotites). Clinopyroxene-orthopyroxene temperatures were calculated only for pyroxenes believed to be in equilibrium (see Fig. 3b, Table 4).

Dawson *et al.* (1997) showed that pyroxenes in the garnet coronas record higher temperatures (reflected in high CaO and Al_2O_3), suggesting that the breakdown of garnet may have been enhanced by heating. Because the coronal clinopyroxenes were often too small to analyze, we calculated the temperature of the coronal assemblages using the amount of Ca in orthopyroxene as a thermometer, which is based on the narrowing of the pyroxene solvus with increasing temperature (Brey and Köhler, 1990). For internal consistency, we simultaneously calculated the temperatures of the groundmass orthopyroxenes by this method. Although the absolute temperatures estimated using this thermometer are uncertain, the relative temperature difference is likely to be robust. A 100-200 °C heating is implied by our calculations. The presence of higher CaO rims on some primary orthopyroxenes in Labait samples also suggests heating.

As shown in Fig. 5, cratonic mantle presently exists to depths of at least 150 km beneath Labait. The Labait peridotites plot above the 41 mW/m² geotherm denoted by Kaapvaal low temperature garnet peridotites and also appear somewhat hotter than Lashaine peridotites which show a large scatter; the Labait peridotites follow a 50 mW/m² geotherm. The Tanzanian craton is characterized by low surface heat flow (23-47 mW/m²) (Nyblade *et al.*, 1990), which is inconsistent with the elevated temperatures recorded by the Labait xenoliths. These temperatures may represent recent thermal effects due to heating from the East African Rift magmas, which are not yet reflected in the surface heat flow.

8. DISCUSSION

8.1 Comparison to Kaapvaaal

Based on petrochemical studies of the Siberian and South African cratons, it is believed that cratonic mantle is highly refractory and variably enriched in silica; the latter is manifested in the orthopyroxene-rich character of Kaapvaal (Boyd, 1989a) and Udachnaya peridotites (Boyd *et al.*, 1997). Like other cratonic mantle, the Tanzanian mantle is also refractory and slightly silica-enriched (Fig. 6). The degree of Si-enrichment, however, is not as large as beneath Kaapvaal (Boyd, 1989a), and more closely resembles the enrichment seen in Siberian peridotites (Boyd *et al.*, 1997). Lashaine peridotites also show moderate silica-enrichment (Rudnick *et al.*, 1994). Interestingly, most of the Labait garnet-bearing peridotites plot closer to the "oceanic trend" and hence show no silica-enrichment. A discussion of the many models proposed to explain silica-enrichment is beyond the scope of this paper. However, we note that peridotites from Somerset Island on the Canadian craton have turned out to be orthopyroxene poor (Schmidberger and Francis, 1997) as well as peridotites from East Greenland (Bernstein *et al.*, 1998). Clearly, the pattern of silica-enrichment in cratonic mantle is complex, and Kaapvaal appears to be one end-member of a spectrum.

8.2 Compositional stratification and implications for the origin and stability of cratonic mantle

The most important finding of this study is that the Tanzanian lithosphere, at least beneath Labait, is compositionally stratified. Indices of fertility, such as FeO, CaO, Al_2O_3, and modal clinopyroxene correlate positively with temperature (Fig. 4d-f). Ni

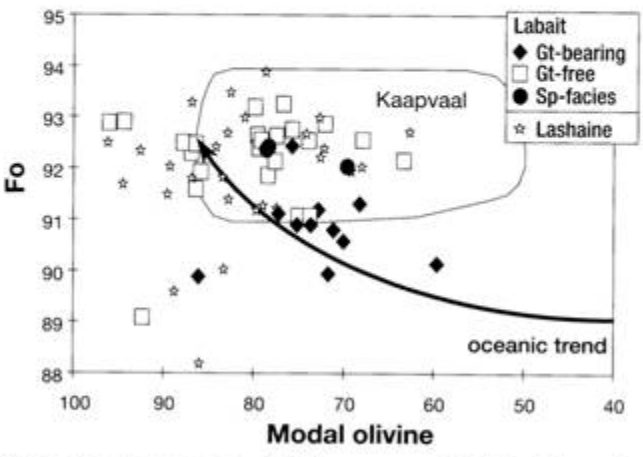

Figure 6. Forsterite content of olivine versus modal olivine. Kaapvaal field and oceanic trend taken from Boyd (1989). Lashaine data taken from Rudnick *et al.* (1994).

(Lee and Rudnick, unpublished data), modal olivine, and Mg/Si correlate negatively with temperature. Fertility increases in a step-wise fashion with depth (Fig. 4d-f). As discussed earlier, a few samples bear evidence for Fe-enrichment; these samples represent small perturbations to the overall compositional stratigraphy of the mantle section (Fig. 4f).

The origin of this compositional stratification is unclear. If the stratification is a primary feature, then it represents a downward decrease in the degree of partial melting, as would be expected for an adiabatic melting column such as in a rising plume. If so, then the compositional trends shown in Fig. 4 are related to partial melting. We found that the model melting curves of Asimow (1998) provided the best-fit to our data (Fig. 4). These residue curves are for relatively low pressure, polybaric batch melting (assuming beginning of melting at 2.5 GPa), which approximates equilibrium porous flow (Asimow, 1998). Considerable deviation from this model, however, is seen for FeO versus MgO (Fig. 4c), which we attribute to the pressure sensitivity of FeO and to the fact that most of the Tanzanian peridotites probably formed at greater pressures than the model is calculated for. Batch melting at 7 GPa (Walter, 1998a and b) apparently depletes the residue of FeO more effectively than melting at lower pressures, which is typical of mid-ocean ridge basalt genesis. Regardless of which melting model is chosen, it is clear that our samples are ultra-refractory, having had 30 to 50 % melt extracted from them.

In a companion study (Chesley *et al.*, 1998), it was shown that spinel-facies peridotites and garnet-free peridotites record approximately the same Re depletion event (~ 2.8 Ga). Because the garnet-free peridotites are believed to have equilibrated at greater depths, the coincident ages suggest that the lithospheric mantle down to depths of ~120 km beneath Labait may have formed during one melting event. However, most of the garnet-bearing peridotites, which are the deepest xenoliths, have younger Re depletion ages. This may reflect their formation from a more recent partial melting event during the Proterozoic or overprinting of the deepest lithosphere (Chesley *et al.*, 1998).

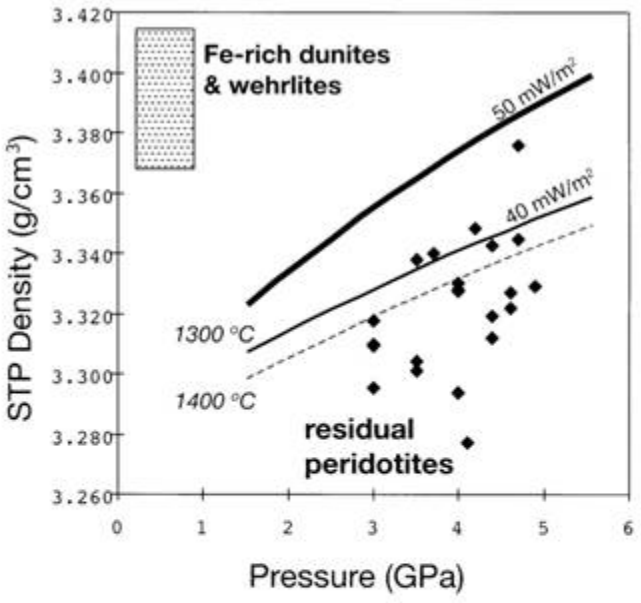

Figure 7. Densities of Labait xenoliths at standard temperature and pressure conditions. Pressures for garnet-free peridotites estimated from their equilibration temperatures and by assuming a conductive geotherm. Isopycnic curves for various lithospheric geotherms calculated using an asthenosphere with potential temperatures of 1300 °C (solid lines) and 1400 °C (dashed line), an adiabatic temperature gradient of 0.5 °C/km, a constant thermal expansivity of 2.7 x 10^{-5}/K, and a density of 3.390 g/cm^3. Lithospheric geotherm models are from Rudnick *et al.* (1998). Densities that lie below isopycnic lines represent stable conditions. Range of densities for Fe-rich dunites and wehrlites at STP are shown by the gray bar.

The downward increase in fertility is equivalent to an increase in intrinsic density. We calculated densities using published densities of mineral end-members, their proportions, and modes. We obtained an average density for the residual peridotites of 3.327 g/cm^3 with deeper, garnet-bearing, samples having densities up to 3.350. For comparison, the average density of Kaapvaal garnet lherzolites is estimated to be 3.353 (Jordan, 1978), identical to that of the deepest portion of the Tanzanian lithosphere. This density is believed to be enough to counteract the negative buoyancy imposed by the cooler thermal state of cratonic mantle according to Jordan's isopycnic hypothesis (1978). We have illustrated this concept graphically in Fig. 7. In order to maintain stability, the density of the cratonic mantle at every level should be less than or equal to that of the surrounding asthenospheric mantle. In Fig. 7, isopycnic curves, representing neutral buoyancy, are shown with densities of residual peridotites at standard temperature and pressure conditions. These curves were calculated for different lithospheric thermal states and for an asthenosphere with a potential temperature of 1300 and 1400 °C, an adiabatic temperature gradient of 0.5 °C/km, and an intrinsic density of 3.390 g/cm^3. Pressures for garnet-free samples have been inferred from equilibration temperatures and a conductive geotherm. It is clear that the residual peridotites from the Tanzanian mantle are dynamically stable at all levels, hence confirming Jordan's isopycnic hypothesis. The occurrence of Archean and Proterozoic mantle beneath Labait as deduced from Re-Os isotope studies (Chesley *et al.*, 1998) attests to the preservation of cratonic mantle despite proximity to rifting. A recent seismic tomographic study has shown that fast shear-wave anomalies extend to depths in excess of 250 km beneath the center of the Tanzanian craton and to depths of ~150-200 km beneath Labait (Ritsema *et al.*, 1998), consistent with the observation that the Tanzanian cratonic mantle persists, despite proximity to rifting.

8.3 The effects of rifting on cratonic mantle

Although this and a companion study (Chesley *et al.*, 1998) have shown that the Tanzanian lithosphere has remained intact since the Precambrian, it has not remained unmodified. Interaction with asthenospheric melts has led to an increase in density of the mantle section by local Fe-enrichment and by formation of Fe-rich dunites. Local Fe-enrichment is geochemically manifested as perturbations to the overall trend of increasing fertility with depth (Fig. 4f), and petrologically manifested in rocks that have low whole-rock Mg# but which have an otherwise depleted composition (low Ca and Al contents). Addition of Fe-rich materials is evidenced by the fact that 75% of the xenolith suite is composed of Fe-rich dunites. It is unclear whether these Fe-rich dunites are the fractional crystallization products of a melt or whether they are products of melt-rock reaction. The fact that most of these have Os and Ni contents similar to residual peridotites (Chesley *et al.*, 1998; Lee and Rudnick, unpublished data) favours the latter hypothesis. Many of the Fe-rich dunites are probably related to Cenozoic rifting, but it is possible that some are related to much older events. Future Re-Os work on Fe-rich samples will shed light on this matter.

The formation of Fe-rich dunites is likely to be the dominant mechanism for increasing the overall density at a given depth.

Their range of densities are shown in Fig. 7. Fe-rich dunites are 0.6 to 3 % denser than residual peridotites. Given the range in densities, a minimum of 25 % addition of Fe-rich dunites via dikes or veins is required for a layer of the mantle to become negatively buoyant. Considering that Fe-rich dunites make up 75 % of the xenoliths in the field, it is possible that the above threshold will or has been met. Therefore, we speculate that as the base of the mantle section beneath Tanzania continues to interact with rift-related magmas, generating dense Fe-rich dunites, it will eventually become negatively buoyant and delaminate, aiding in the mechanical thinning of the lithosphere. The presence of low seismic shear wave velocities at depths >150 km beneath Labait suggests that the effects of rifting are currently propagating into the craton's margin (Ritsema *et al.*, 1998). These low seismic velocities may be manifestations of elevated temperatures and/or the presence of dense Fe-rich bodies.

9. SUMMARY

1) Tanzanian cratonic mantle extends to depths of at least 150 km beneath the Labait volcano in the Tanzanian section of the East African Rift. Re-Os systematics indicate that the upper 120 km formed during the Archean while the lowermost lithospheric section was either overprinted or formed during the Proterozoic (Chesley *et al.*, 1998).
2) Tanzanian cratonic mantle is compositionally stratified, with a step-wise increase in fertility with depth.
3) Density calculations indicate that the residual peridotites satisfy the isopycnic hypothesis and are thus dynamically stable with respect to the asthenosphere. This interpretation is supported by the preservation of Archean and Proterozoic Re-Os depletion ages beneath Labait.
4) Xenoliths record elevated temperatures at depth, and some samples have experienced Fe-enrichment. Thus the mantle section has been chemically and thermally modified. Some of these modifications are due to Cenozoic rifting and some may be older.
5) Fe-rich peridotites make up 75% of the xenolith suite in the field, and are much denser than the residual peridotites. The contribution of Fe-rich dunites via dikes, veins, or reaction zones to layers of residual peridotite may eventually impose negative buoyancy, causing such layers to delaminate.

ACKNOWLEDGEMENTS

This research was supported by an NSF graduate fellowship to C.-T. Lee and by NSF grant (EAR 9506510) to R. L. Rudnick and J. Chesley. We are indebted to A. Tesha for help in the field, the crew of Dorobo Safaris for making fieldwork possible, the Tanzanian government for allowing us to collect samples, C. Carman and D. Lange for help in electron microprobe analyses, and K. Tomford for bearing most of the dirty work (sample preparation). We also benefited from valuable discussions with P.D. Asimow, M. Barth, T. Battenhouse, J. Chesley, B. Dawson, I. Horn, S. Jacobsen, S. Master, W.F. McDonough, A. Nyblade, D. Smith, K. Tainton, and M.J. Walter. We are grateful to P. Asimow and M.J. Walter for allowing the use of preprint material. Lastly, we acknowledge our fortune for being involved in the MIT-Harvard joint seminar and workshop on continental roots held in 1997, which provided a fertile environment for development of some of the ideas presented here.

REFERENCES

ALLEGRE C.J., POIRIER J.-P., HUMLER E. & HOFMANN A.W., 1995. The chemical composition of the Earth. *Earth Planet. Sc. Lett.* **134,** pp. 515-526.

ASIMOW P.D., 1998. A model that reconciles major- and trace-element data from abyssal peridotites. submitted to *Earth Planet. Sc. Lett.*

BORG G. & SHACKLETON R.M., 1997. The Tanzania and NE-Zaire cratons. In DeWit, M. J. and L. D. Ashwal eds., *Greenstone Belts.* Oxford University Press, Oxford, pp. 608-619.

BERNSTEIN S., KELEMEN P.B. & BROOKS C.K., 1998. Depleted spinel harzburgite xenoliths in Tertiary dykes from East Greenland: Restites from high degree melting. *Earth Planet. Sc. Lett.* **154,** pp. 221-235.

BODINIER J.-L., MERLET C., BEDINI R.M., SIMIEN F., REMAIDI M. & GARRIDO C.J., 1996. Distribution of niobium, tantalum, and other highly incompatible trace elements in the lithospheric mantle: The spinel paradox. *Geochim. Cosmochim. Acta.* **60,** pp. 545-550.

BOYD F.R., 1989a. Compositional distinction between oceanic and cratonic lithosphere. *Earth Planet. Sc. Lett.* **96,** pp. 15-26.

BOYD F.R., 1989b. Kaapvaal spinel peridotites: evidence of craton origin. *Yearbook-Carnegie. Inst. Wash.*, p. 3-6.

BOYD F.R., POKHILENKO N.P., PEARSON D.G., MERTZMAN S.A., SOBOLEV N.V. & FINGER L.W., 1997. Composition of the Siberian cratonic mantle: evidence from Udachnaya peridotite xenoliths. *Contrib. Mineral. Petrol.* **128,** pp. 228-246.

BREY G.P. & KÖHLER T., 1990. Geothermobarometry in four-phase lherzolites II. New thermobarometers, and practical assessment of existing thermobarometers. *Journ. Petrol.* **31,** pp. 1353-1378.

CHESLEY J., RUDNICK R.L. & LEE C.-T., 1998. Re-Os systematics of mantle xenoliths from the East African Rift: evidence for longevity of the cratonic mantle and Os metasomatism, submitted to *Geochim. Cosmochim. Acta.*

DAUTRIA J.M., DUPUY C., TAKHERIST D. & DOSTAL J., 1992. Carbonate metasomatism in the lithospheric mantle: peridotitic xenoliths from a melilititic district of the Sahara basin: *Contrib. Mineral. Petrol.* **111,** pp. 37-52.

DAWSON J.B., 1992. Neogene tectonics and volcanicity in the North Tanzania sector of the Gregory Rift Valley: contrasts with the Kenya sector. *Tectonophys.* **204,** pp. 81-92.

DAWSON J.B., JAMES D., PASLICK C. & HALLIDAY A.M., 1996. Ultrabasic potassic low-volume magmatism and continental rifting in north-central Tanzania: association with enhanced heat flow. *Russian Geol. Geophys.* **38,** pp. 69-81.

DAWSON J.B., 1998. Metasomatism and melting in spinel peridotite xenoliths from Labait, Tanzania. *(This volume.)*

EBINGER C., POUDJOM DJOMANI Y., MBEDE E., FOSTER A. & DAWSON J.B., 1997. Rifting Arcaean lithosphere: the Eyasi-Manyara-Natron rifts, East Africa. *Journ. Geol. Soc. London* **154,** pp. 947-960.

ERLANK A.J., WATERS F.G., HAWKESWORTH C.J., HAGGERTY S.E., ALLSOPP H.L., RICKARD R.S. & MENZIES M., 1987. Evidence for mantle metasomatism in peridotite nodules from the Kimberly pipes, South Africa. In Menzies, M. and Hawkesworth, C. J., eds., *Mantle metasomatism.* Academic Press, London, pp. 221-311.

FOSTER A., EBINGER C., MBEDE E. & REX D., 1997. Tectonic development of the northern Tanzanian sector of the East African Rift System. *Journ. Geol. Soc. London* **154,** pp. 689-700.

HUNTER R.H. & TAYLOR L.A., 1982. Instability of garnet from the mantle: glass as evidence of metasomatic melting. *Geology* **10,** pp. 617-620.

JAQUES A.L., O'NEILL H.ST.C., SMITH C.B., MOON J. & CHAPPELL B.W., 1990. Diamondiferous peridotite xenoliths from the Argyle (AK1) lamproite pipe, Western Australia. *Contrib. Mineral. Petrol.* **104,** pp. 255-276.

JORDAN T.H., 1978. Composition and development of the continental tectosphere. *Nature* **274,** pp. 544-548.

JORDAN T.H., 1988. Structure and formation of the continental tectosphere. *Journ. Petrol. Special Lithosphere Issue,* pp. 11-37.

LEE C.-T. & RUDNICK R.L., 1998. Magmatic calcite in peridotite xenoliths from Tanzania: *EOS Trans. Amer. Geophys. Un.* **79,** pp. 354.

MCDONOUGH W.F., 1990. Constraints on the composition of the continental lithospheric mantle. *Earth Planet. Sc. Lett.* **101,** pp. 1-18.

MCDONOUGH W.F. & S.-S. SUN., 1995. The composition of the Earth. *Chem. Geol.* **120,** pp. 223-253.

MERCIER J.-C.C., 1985, Olivine and pyroxnes. In Wenk, H.-R., ed., *Preferred Orientation in Deformed Metals and Rocks: An Introduction to Modern Texture Analysis.* Academic Press, London, pp. 407-430.

MÖLLER A., APPEL P., MEZGER K. & SCHENK V., 1995. Evidence for a 2 Ga subduction zone: eclogites in the Usagaran belt of Tanzania. *Geology* **23,** pp. 1067-1070.

MÖLLER A., MEZGER K. & SCHENK V., 1998. Crustal age domains and the evolution of the continental crust in the Mozambique belt of Tanzania: Combined Sm-Nd, Rb-Sr, and Pb-Pb isotopic evidence. *Journ. Petrol.* **39,** pp. 749-783.

NYBLADE A.A., POLLACK H.N., JONES D.L., PODMORE F. & MUSHAYANDEBVU M., 1990. Terrestrial heat flow in east and southern Africa. *Journ. Geophys. Res.* **95,** pp. 17371-17384.

O'NEILL H.ST.C., 1981. The transition between spinel lherzolite and garnet lherzolite, and its use as a geobarometer. *Contrib. Mineral. Petrol.* **77,** pp. 185-194.

PEARSON D.G., CARLSON R.W., SHIREY S.B., BOYD F.R. & NIXON P.H., 1995. Stabilisation of Archaean lithospheric mantle: A Re-Os isotope study of peridotite xenoliths from the Kaapvaal craton. *Earth Planet. Sc. Lett.* **134,** pp. 341-357.

PIKE J.E.N., MEYER C.E. & WILSHIRE H.G., 1980. Petrography and chemical composition of a suite of ultramafic xenoliths from Lashaine, Tanzania. *Journ. Geol.* **88,** pp. 343-352.

PINNA P., COCHERIE A., THIEBLEMONT D., FEYBESSE J.-L. & LAGNY P., 1996. Evolution geodynamique du craton est-Africain et determinisme gitologique: *Chronique de la recherche miniere* **525,** pp. 33-43.

REID A.M. & DAWSON J.B., 1972. Olivine-garnet reaction in peridotites from Tanzania. *Lithos* **5,** pp. 115-124.

RICHARDSON S.H., GURNEY J.J., ERLANK A.J. & HARRIS J.W., 1984. Origin of diamonds in old enriched mantle. *Nature* **310,** pp., 198-202.

RINGWOOD A.E., 1966. The chemical composition and origin of the Earth. *Advances in Earth Science.* M.I.T. Press, pp. 287-356.

RITSEMA J., NYBLADE A.A., OWENS T.J., LANGSTON C.A. & VANDECAR J.C., 1998. Upper mantle seismic velocity structure beneath Tanzania, East Africa: implications for the stability of cratonic lithosphere. *Journ. Geophys. Res.* **103,** pp. 21201-21213.

RUDNICK R.L., IRELAND T.R., GEHRELS G., IRVING A.J., CHESLEY J.T. & HANCHAR J.M., 1998. Dating mantle metasomatism: U-Pb geochronology of zircons in cratonic mantle xenoliths from Montana and Tanzania. *(This volume.)*

RUDNICK R.L., MCDONOUGH W.F. & CHAPPELL B.W., 1993. Carbonatite metasomatism in the northern Tanzanian mantle: petrographic and geochemical characteristics. *Earth Planet. Sc. Lett.* **114,** pp. 463-475.

RUDNICK R.L., MCDONOUGH W.F. & ORPIN A., 1994. Northern Tanzanian peridotite xenoliths: a comparison with Kaapvaal peridotites and inferences on metasomatic interactions. In Meyer, H. O. A. and Leonards, O. H. eds., *Kimberlites, related rocks and mantle xenoliths.* Proc. Fifth Int. Kimberlite Conf. 1, CPRM Spec. Publ. 1A, Brasilia, pp. 336-353.

RUDNICK R.L., MCDONOUGH W.F. & O'CONNELL R.J., 1998. Thermal structure, thickness and composition of continental lithosphere. *Chem. Geol.* **145,** pp. 395-411.

SCHMIDBERGER S.S. & FRANCIS D., 1997. Hf isotopic evidence for Cretaceous modification of cratonic mantle roots beneath northern Canada: a study of mantle xenoliths from Somerset Island kimberlites. *Amer. Geophys. Union Fall Abstr.* **78,** pp. 749.

SMITH D., 1977. The origin and interpretation of spinel-pyroxene clusters in peridotite. *Journ. Geol.* **85,** pp. 476-482.

SMITH D. & WILSON C.R., 1985. Garnet-olivine equilibration during cooling in the mantle. *Am. Mineral.* **70,** pp. 30-39.

WALKER R.J., CARLSON R.W., SHIREY S.B. & BOYD F.R., 1989. Os, Sr, Nd, and Pb isotope systematics of southern African peridotite xenoliths: implications for the chemical evolution of subcontinental mantle. *Geochim. Cosmochim. Acta* **53,** pp. 1583-1595.

WALTER M.J., 1998a. Melting of garnet peridotite and the origin of komatiite and depleted lithosphere. *Journ. Petrol.* **39,** pp. 29-60.

WALTER M.J., 1998b. Melting residues of garnet peridotite and the origin of cratonic lithosphere. In Fei, Y.-W, Bertka, C.B & Mysen, B. eds. *Mantle Petrology: field observations and high pressure experimentation,* Geochem. Soc. (in press).

YAMADA H. & TAKAHASHI E., 1984. Subsolidus phase relations between coexisting garnet and two pyroxenes at 50 to 100 kbar in the system CaO-MgO-Al_2O_3-SiO_2. In Kornprobst, J. *Kimberlites II. The mantle and crust-mantle relationships.* Proc. Third Int. Kimberlite Conf., Elsevier, Amsterdam, pp. 247-249.